BENNETT

AI-POWERED BIOLOGICAL INTELLIGENCE

IDENTIFYN RESOLUTION STEPDOWN

ATR.P

MICROSCOPY EVIDENCE ASSESSMENT

Rabbit anti-Human ATR.p (Threonine 1989) Recombinant Monoclonal

WESTERN BLOT -> WIDEFIELD -> WIDEFIELD SIM / APOTOME -> CONFOCAL -> AIRYSCAN
SIM -> SIM² -> SINGLE-MOLECULE STORM

8	1	PENDING
ORDERED EVIDENCE TIERS	SUPPORTING CONTROL	SCIENTIST REVIEW

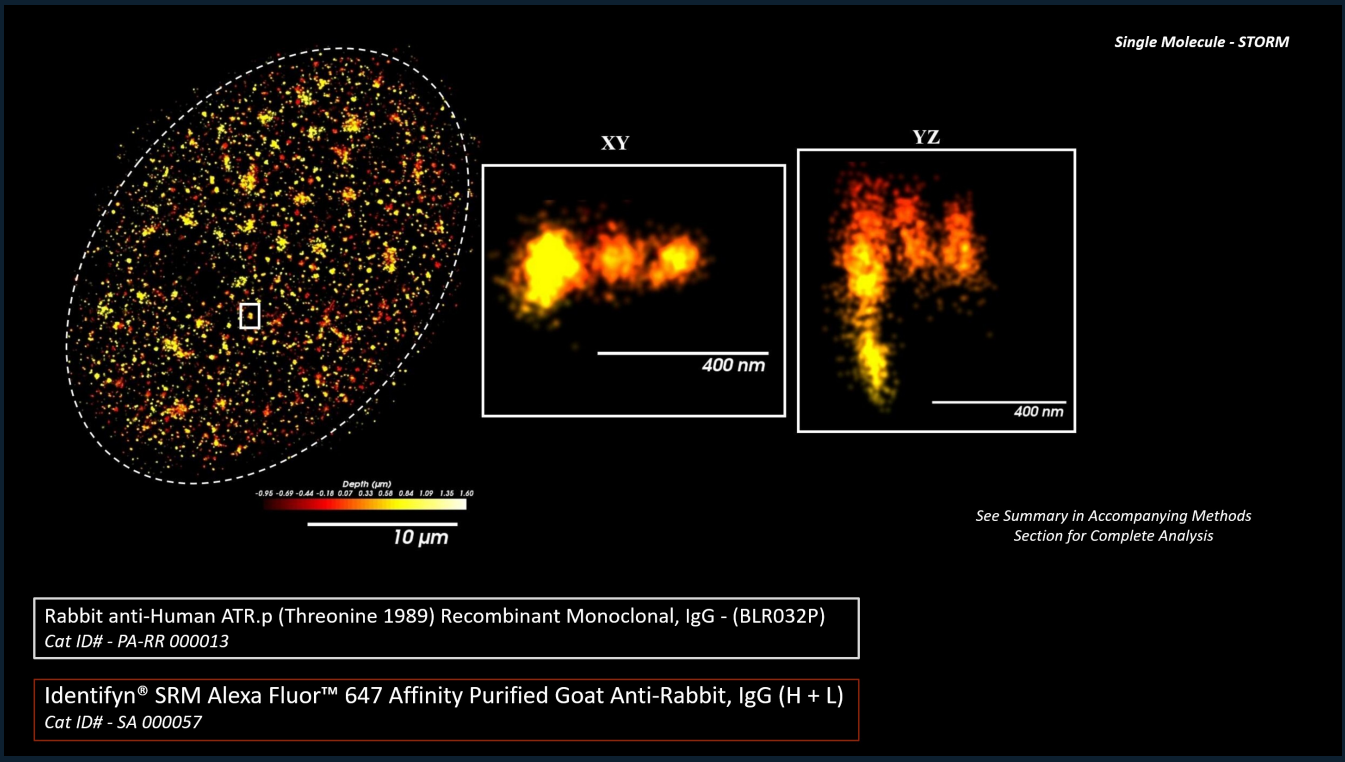

REPRESENTATIVE HIGHEST-AVAILABLE VIEW / SINGLE-MOLECULE STORM

PA-RR-000013 | PRODUCT-LEVEL EVIDENCE DOSSIER

SOURCE-GROUNDED MICROSCOPY + BIOLOGICAL REVIEW / IDENTIFYN EVIDENCE PRESERVED

UNPUBLISHED / PENDING SCIENTIST REVIEW / NO PUBLICATION AUTHORIZED

CRO CAPABILITY DEMONSTRATED

Identifyn performed the experimental and imaging work documented below. BENNETT converts that operating history into a governed, source-bounded scientific record.

- Sample preparation and immunofluorescence staining
- Antibody/reagent performance documentation
- Etoposide treatment / DNA-damage model
- Western blot
- Widefield
- Widefield SIM — Apotome
- Confocal
- Airyscan
- SIM
- SIM²
- Single-molecule STORM
- 3D / Z-stack acquisition
- Multi-channel microscopy
- Spatial / localization analysis
- Intensity analysis
- Control experiment
- BENNETT governed evidence assessment

SCIENTIFIC QUESTION

How does ATR.p(T1989)-attributed signal and its spatial relationship to the companion damage-response channel change in the displayed full Stepdown record?

EVIDENCE AVAILABLE

Western blot -> Widefield -> Widefield SIM — Apotome -> Confocal -> Airyscan -> SIM -> SIM² -> Single-molecule STORM -> Control

BENNETT ASSESSMENT

This full Stepdown record demonstrates the broadest integrated CRO workflow in the pilot, from Western blot through STORM. The displayed evidence supports a source-bounded spatial progression, not direct ATR-gammaH2AX interaction, pathway causation or native-data molecular measurement.

BENNETT / MICROSCOPY AND BIOLOGICAL EVIDENCE REVIEW

SOURCE-GROUNDED RETROSPECTIVE REVIEW / PENDING SCIENTIST REVIEW

SOURCE STATE	SOURCE HASH VERIFIED / EVENT RECORDED
BENNETT EVIDENCE REVIEW	COMPLETED / SOURCE-BOUNDED
NATIVE IMAGE REPROCESSING	NOT PERFORMED
LITERATURE SOURCES	INDEPENDENTLY VERIFIED
SCIENTIST REVIEW	PENDING
PUBLICATION	NOT AUTHORIZED

OVERALL CALL / BIOLOGICALLY CONSISTENT / NOT INDEPENDENTLY VALIDATED

Across the preserved presentations, phospho-ATR(T1989)-attributed signal is predominantly nuclear and punctate after etoposide exposure, with recurrent spatial coincidence - but not equivalence or proven interaction - with gamma-H2AX-marked nuclear regions. Higher-resolution tiers display increasing separation of punctate and irregular substructure. The pattern is consistent with published damage-regulated ATR T1989 phosphorylation and etoposide-associated gamma-H2AX responses, but the package does not independently establish antibody specificity, direct interaction, causation, exact resolution or nanoscale molecular organization.

SETTINGS ASSESSMENT

The source documents a complete ordered Stepdown from direct-lysate Western blot through widefield, optical sectioning, confocal, Airyscan, SIM, SIM2 and STORM, followed by the treated/untreated control. BENNETT uses each modality's documented acquisition and processing context and does not treat the series as a quantitative intensity ladder.

BIOLOGICAL SUPPORT

BENNETT can correlate the visible nuclear damage-associated pattern with published ATR and gamma-H2AX biology. Its strongest safe statement is consistency: the observations fit the known response, but do not prove target identity, molecular interaction, pathway causation, clinical meaning or generality beyond the displayed source record.

CONTROL ASSESSMENT

The source-selected treated region has higher reported maximum and mean fluorescence than the source-selected untreated region. This direction agrees with the literature, but the presentation lacks the replication and statistics required for a population-level effect claim.

CLAIM CEILING

The preserved PA-RR-000013 record is biologically and technically consistent with an etoposide-associated phospho-ATR(T1989) damage-response pattern and progressive visualization of nuclear substructure across modalities. It is not an independent validation of reagent specificity, direct ATR-gamma-H2AX interaction, ATR causation of H2AX phosphorylation, numerical resolution, molecule count, cluster identity or mechanism.

PROCESSING DISCLOSURE

Retrospective BENNETT evaluation of preserved Identifyn presentation images, source-reported results, documented settings and independently verified primary literature. BENNETT did not reprocess native image files or repeat the historical measurements. Reconciled metadata values are derivative QA determinations from internal record consistency, not new image measurements.

REAGENTS AND ACQUIRED CHANNELS

Preparation reagents are reported separately from channels actually documented in the acquisition settings. Fluorophores mentioned in staining are not automatically treated as acquired channels.

EVIDENCE OBJECT	REAGENTS / FLUOROPHORES PRESENT	CHANNELS ACTUALLY ACQUIRED
Western blot	647	NOT APPLICABLE - scanner detection record
Widefield	405/DAPI; 488; 647	PASS - ACQUISITION ENTRIES CONSISTENT; 3 channel(s); Reflector: 50 Cy 5 | 38 eGFP | 49 DAPI
Widefield SIM — Apotome	405/DAPI; 488; 647	PASS - ACQUISITION ENTRIES CONSISTENT; 3 channel(s); Reflector: 50 Cy 5 | 38 eGFP | 49 DAPI
Confocal	405/DAPI; 488; 647	PASS - ACQUISITION ENTRIES CONSISTENT; 3 channel(s); Laser Wavelength: 639 nm @ 1.8% | 488 nm @ 0.2% | 405 nm @ 0.2%
Airyscan	405/DAPI; 488; 647; 750	PASS - ACQUISITION ENTRIES CONSISTENT; 3 channel(s); Laser Wavelength: 639 nm @ 2.60% | 488 nm @ 0.3% | 405 nm @ 0.3%
SIM	405/DAPI; 488; 647	UNRESOLVED - CONFLICTING ACQUISITION BLOCK COUNTS; declared channel counts: [2, 3]; Laser Wavelength: 640 nm @ 3.5% | 488 nm @ 0.50%; Excitation Wavelength: 640 | 488; Imaging Device: Axiocam 820
SIM²	405/DAPI; 488; 647	UNRESOLVED - CONFLICTING ACQUISITION BLOCK COUNTS; declared channel counts: [2, 3]; Laser Wavelength: 640 nm @ 3.5% | 488 nm @ 0.50%; Excitation Wavelength: 640 | 488; Imaging Device: Axiocam 820
Single-molecule STORM	647	PASS - ACQUISITION ENTRIES CONSISTENT; 1 channel(s); Color Channel: Both Channels
Control	405/DAPI; 488; 647	PASS - ACQUISITION ENTRIES CONSISTENT; 1 channel(s); Laser Wavelength: 639 nm @ 1.8%

MODALITY ASSESSMENT / PART 1 OF 9

Western blot / BOUNDED CORRELATION / SCIENTIST REVIEW REQUIRED

DOCUMENTED SETTINGS

Direct HeLa nuclear-lysate blot after 2 uM etoposide for 20 h; expected target size 301 kDa; Azure Sapphire FL, 638 nm excitation, 676 +/- 37 nm emission, PMT detection; no source-reported post-processing.

VISIBLE OBSERVATION

The preserved presentation shows untreated (-) and etoposide-treated (+) lanes and a visibly stronger high-molecular-weight fluorescent band in the treated lane.

SOURCE-REPORTED RESULT

The source identifies the band as phospho-ATR(T1989) near the expected 301 kDa region. This is a source attribution, not a new BENNETT identity measurement.

LITERATURE CORRELATION

Published work supports damage-regulated ATR T1989 phosphorylation as a proximal marker of active ATR signaling.

INTERPRETIVE LIMIT

Band position and treatment response alone do not establish antibody specificity. The foundational phospho-T1989 study reported a near-molecular-weight cross-reacting band when immunoblotting without ATR immunoprecipitation, which is directly relevant to this direct-lysate presentation.

CLAIM CEILING

The blot is consistent with an etoposide-associated increase in a high-molecular-weight signal attributed by the source to phospho-ATR(T1989); it does not independently prove band identity or analytical specificity.

MODALITY ASSESSMENT / PART 2 OF 9

Widefield / BOUNDED CORRELATION / SCIENTIST REVIEW REQUIRED

DOCUMENTED SETTINGS

Zeiss Axio Imager.M1; 63x/1.40 oil objective; Axiocam 705; 0.110 um pixels; DAPI, AF488 and AF647 channels; source-reported exposures of 100-300 ms.

VISIBLE OBSERVATION

The displayed cells contain predominantly nuclear punctate red and green signals. The merge includes yellow/orange regions where the two displayed channels overlap at widefield resolution.

SOURCE-REPORTED RESULT

The source reports an ROI-based colocalization view for two nuclei and interprets the pattern as damage-associated phospho-ATR and gamma-H2AX signal overlap.

LITERATURE CORRELATION

Etoposide is established to induce gamma-H2AX-associated DNA-damage responses, and ATR T1989 phosphorylation is damage regulated. The displayed nuclear pattern is therefore biologically consistent with the source treatment and labels.

INTERPRETIVE LIMIT

Pixel overlap is not proof of molecular binding, direct interaction, shared molecular identity, or ATR-dependent phosphorylation of H2AX. Widefield blur can merge nearby but distinct structures.

CLAIM CEILING

The image supports nuclear, punctate, spatially coincident signal at diffraction-limited scale; it does not establish direct ATR-gamma-H2AX interaction or nanoscale colocalization.

MODALITY ASSESSMENT / PART 3 OF 9

Widefield SIM - Apotome / BOUNDED CORRELATION / SCIENTIST REVIEW REQUIRED

DOCUMENTED SETTINGS

Zeiss Axio Observer.Z1/7 Apotome; 63x/1.25 oil objective; 0.143 x 0.143 x 0.100 um sampling; 47-85 source-reported Z slices; optical-sectioning correction enabled; deconvolution not used.

VISIBLE OBSERVATION

The 3D presentation and orthogonal/clipped views show red and green signal distributed within the nuclear volume, with recurrent areas of spatial overlap and areas that remain separate.

SOURCE-REPORTED RESULT

The source interprets the overlap as coordinated recruitment within damage-associated nuclear territories and explicitly stops short of definitive molecular colocalization.

LITERATURE CORRELATION

The nuclear distribution is consistent with damage-associated ATR signaling and gamma-H2AX-marked chromatin territories described in the literature.

INTERPRETIVE LIMIT

Apotome optical sectioning improves background rejection and axial presentation but is not equivalent to reconstructed super-resolution. The presentation does not establish physical interaction.

CLAIM CEILING

The record supports three-dimensional nuclear co-occurrence at the scale of the optical-sectioned presentation, not molecular association.

MODALITY ASSESSMENT / PART 4 OF 9

Confocal / BOUNDED CORRELATION / SCIENTIST REVIEW REQUIRED

DOCUMENTED SETTINGS

Zeiss LSM980; 63x/1.40 oil objective; 151 source-reported Z slices at 0.030 um spacing; 1 AU pinholes; GaAsP-PMT; 639 and 488 nm excitation; eightfold averaging.

VISIBLE OBSERVATION

The optical-section presentation shows discrete nuclear red and green puncta. A displayed line profile contains partially aligned channel peaks across the selected path.

SOURCE-REPORTED RESULT

The source reports spatial concordance in its selected line profile and describes overlapping damage-associated signaling territories.

LITERATURE CORRELATION

The observation is compatible with two damage-response labels occupying some of the same nuclear regions after etoposide exposure.

INTERPRETIVE LIMIT

The plotted profile is source-reported and was not recomputed by BENNETT. A single selected line and presentation image do not provide population statistics, interaction evidence, or cross-modality intensity equivalence.

CLAIM CEILING

The record supports partial spatial concordance within the displayed optical section and selected source line profile, bounded to that presentation and ROI.

MODALITY ASSESSMENT / PART 5 OF 9

Airyscan / BOUNDED CORRELATION / SCIENTIST REVIEW REQUIRED

DOCUMENTED SETTINGS

Zeiss LSM980 Airyscan; 63x/1.40 oil objective; 131 source-reported Z slices; Airyscan SuperResolution 3D processing; 639 and 488 nm excitation.

VISIBLE OBSERVATION

The presentation separates the nuclear signal into more distinct red and green puncta than the lower-resolution tiers while retaining some yellow overlap regions.

SOURCE-REPORTED RESULT

The source presents a selected optical section, 3D rendering, and a same-product STORM comparison to illustrate remaining resolution limits.

LITERATURE CORRELATION

Greater apparent feature separation is expected when detector-array sampling and reconstruction improve effective resolution.

INTERPRETIVE LIMIT

Native detector data, calibration and processing QC are absent from this retrospective package. Apparent fine morphology cannot be converted into a numerical resolution claim or molecular interaction claim.

CLAIM CEILING

The presentation supports increased visual separation of punctate nuclear features relative to the lower-resolution displays, without assigning molecular-scale structure.

MODALITY ASSESSMENT / PART 6 OF 9

SIM / BOUNDED CORRELATION / SCIENTIST REVIEW REQUIRED

DOCUMENTED SETTINGS

Zeiss Elyra 5 Lattice SIM; 63x/1.40 oil objective; 115 source-reported Z slices; 0.030 um Z spacing; 120 ms exposure; 3D SIM reconstruction with automatic sharpness.

VISIBLE OBSERVATION

The presentation resolves finer punctate and elongated nuclear features, with red and green distributions that are sometimes adjacent, sometimes overlapping, and sometimes separate.

SOURCE-REPORTED RESULT

The source characterizes this as increased structural discrimination and compares the displayed field with a same-product STORM inset.

LITERATURE CORRELATION

The direction of change is consistent with SIM resolving features that conventional microscopy blends, while microscopy literature requires reconstruction-specific quality control.

INTERPRETIVE LIMIT

Raw patterned frames, modulation assessment and reconstruction-artifact checks are not available here. Fine structures may be biological, reconstruction dependent, or a mixture of both.

CLAIM CEILING

The presentation supports finer displayed feature separation than lower-resolution tiers; it does not validate exact dimensions, resolution, or molecular architecture.

MODALITY ASSESSMENT / PART 7 OF 9

SIM2 / BOUNDED CORRELATION / SCIENTIST REVIEW REQUIRED

DOCUMENTED SETTINGS

Same Elyra 5 acquisition family as SIM; source-reported iterative SIM2 reconstruction with three iterations, low input-SNR setting, zero regularization weight and no additional filter.

VISIBLE OBSERVATION

The displayed phospho-ATR channel contains more distinct irregular, punctate and elongated signal forms than are apparent in the lower-resolution presentations.

SOURCE-REPORTED RESULT

The source interprets this as further refinement of sub-diffraction structural discrimination and includes a same-product STORM comparison.

LITERATURE CORRELATION

An iterative reconstruction can increase apparent separation of close features, but the biological meaning of the resulting shapes depends on reconstruction fidelity.

INTERPRETIVE LIMIT

Without raw data and artifact review, BENNETT cannot determine which fine forms are specimen structure versus reconstruction behavior.

CLAIM CEILING

The presentation supports a more finely segmented phospho-ATR signal pattern; it does not assign molecular identity, dimensions, or mechanism to the fine forms.

MODALITY ASSESSMENT / PART 8 OF 9

Single-molecule STORM / BOUNDED CORRELATION / SCIENTIST REVIEW REQUIRED

DOCUMENTED SETTINGS

Bruker Vutara VXL biplane system; 60x/1.30 silicon-oil objective; dual-camera workflow; 20 ms super-resolution exposure; drift correction; 200 frames x 4 Z positions x 35 cycles; DBSCAN shown in source method.

VISIBLE OBSERVATION

The localization presentation shows a dense nuclear phospho-ATR map and a magnified XY/YZ region with substructure within an apparent focus or aggregate.

SOURCE-REPORTED RESULT

The source reports localization processing and cluster-analysis settings and interprets the view as nanoscale organization of phospho-ATR-associated structures.

LITERATURE CORRELATION

Localization microscopy can reveal sub-diffraction organization, but published benchmarks show that image quality depends strongly on localization software, model fit and quality control.

INTERPRETIVE LIMIT

The retrospective package does not include localization tables, uncertainty distributions, blinking correction, density controls, drift traces or an independent cluster analysis. Apparent clusters cannot be treated as molecule counts or binding complexes.

CLAIM CEILING

The presentation supports displayed substructure within a selected phospho-ATR localization region; it does not establish molecule number, cluster truth, binding, or exact localization precision.

MODALITY ASSESSMENT / PART 9 OF 9

Control / BOUNDED CORRELATION / SCIENTIST REVIEW REQUIRED

DOCUMENTED SETTINGS

Zeiss LSM980 confocal comparison of etoposide-treated and untreated HeLa preparations; source states matched acquisition parameters for the displayed comparison; 16-bit AF647 phospho-ATR channel.

VISIBLE OBSERVATION

The treated presentation appears more punctate and contains stronger displayed signal than the untreated presentation, which appears lower-intensity and more diffuse.

SOURCE-REPORTED RESULT

The source reports maximum values of 31,292 versus 8,762 and arithmetic means of 702.066 versus 471.197 for its selected treated and untreated regions. BENNETT arithmetic gives treated/untreated ratios of 3.571 for the maxima and 1.490 for the means.

LITERATURE CORRELATION

A higher treated phospho-ATR(T1989)-attributed signal is directionally consistent with published damage-regulated ATR T1989 phosphorylation.

INTERPRETIVE LIMIT

These are source-selected images and regions, not a BENNETT remeasurement or a replicated effect estimate. The record does not provide sample size, variance, blinding, inferential statistics, or independent antibody-specificity validation.

CLAIM CEILING

For the displayed source-selected regions, the treated condition has higher source-reported phospho-ATR-attributed signal. No population-wide magnitude, statistical significance, causation, or specificity claim is authorized.

CROSS-MODALITY SYNTHESIS

The strongest recurring observation is not that every modality proves the same structure. It is that a nuclear punctate signal pattern persists while increasing optical and computational resolution separates previously blended features. That persistence strengthens internal coherence; it does not remove modality-specific artifacts or convert presentation images into native-data validation.

No cross-modality intensity comparison is authorized because acquisition, labeling, detector response, processing and displayed regions differ. Spatial overlap is reported as co-occurrence only. Super-resolution morphology remains provisional without raw-data and reconstruction/localization QC.

BENNETT LITERATURE CORRELATION — SOURCES INDEPENDENTLY VERIFIED

BENNETT uses independently verified primary scientific sources to test whether the interpretation is scientifically consistent and properly bounded. Literature correlation does not retroactively validate the Identifyn dataset or replace scientist review.

- ATR T1989 phosphorylation is damage regulated and has been reported as a proximal marker of ATR activation; a separate primary study describes T1989 autophosphorylation as important to checkpoint activation.

- Etoposide-induced gamma-H2AX is a sensitive marker of DNA damage, but gamma-H2AX does not identify one upstream kinase or prove ATR caused H2AX phosphorylation in this record.

- Fluorescence colocalization can occur without physical interaction; co-occurrence must remain distinct from binding, FRET-scale proximity or mechanism.

- SIM and single-molecule localization outputs depend on reconstruction/localization choices and QC. Presentation images alone cannot validate exact resolution, localization precision, molecule number or cluster truth.

REFERENCES

1. Nam EA, et al. Thr-1989 phosphorylation is a marker of active ATR kinase. J Biol Chem. 2011;286:28707-28714. doi:10.1074/jbc.M111.248914. https://pubmed.ncbi.nlm.nih.gov/21705319/
2. Liu S, et al. ATR autophosphorylation as a molecular switch for checkpoint activation. Mol Cell. 2011;43:192-202. doi:10.1016/j.molcel.2011.06.019. https://pubmed.ncbi.nlm.nih.gov/21777809/
3. Smart DJ, et al. Assessment of DNA double-strand breaks and gammaH2AX induced by etoposide and mitoxantrone. Mutat Res. 2008;641:43-47. doi:10.1016/j.mrfmmm.2008.03.005. https://pubmed.ncbi.nlm.nih.gov/18423498/
4. Moser B, et al. Fluorescence colocalization microscopy analysis can be improved by combining object-recognition with pixel-intensity-correlation. Biotechnol J. 2017;12:1600332. doi:10.1002/biot.201600332. https://pubmed.ncbi.nlm.nih.gov/27420480/
5. Helmuth JA, et al. Beyond co-localization: inferring spatial interactions between sub-cellular structures from microscopy images. BMC Bioinformatics. 2010;11:372. doi:10.1186/1471-2105-11-372. https://pubmed.ncbi.nlm.nih.gov/20609242/
6. Sage D, et al. Quantitative evaluation of software packages for single-molecule localization microscopy. Nat Methods. 2015;12:717-724. doi:10.1038/nmeth.3442. https://www.nature.com/articles/nmeth.3442

RELEASE BOUNDARY

This assessment remains a draft pending scientist review. No publication is authorized. Any future native-file analysis must enter BENNETT as a new evidence snapshot with routed engine authority, native-data QA, methods, limitations, and an independently reviewed claim ceiling.

SOURCE RECONCILIATION / QA / PROVENANCE

SOURCE STATUS - AUTO-RECONCILED

Historical Identifyn source material was subjected to BENNETT retrospective QA. Original source state and correction history remain preserved in provenance.

HIGH CONFIDENCE - AUTO-RECONCILED

Airyscan / Scaling (Per Pixel): 0.035 nm X 0.035 nm X 0.030 nm -> 0.03529 µm X 0.03530 µm X 0.03000 µm. Both numerical magnitude and unit were normalized, then checked against the reported field dimensions; no unit label was changed alone. Supporting evidence: Image Size (Pixels)=731 X 676; Image Size (Scaled)=25.80 µm X 23.86 µm; PASS - INTERNALLY CONSISTENT. The source magnitude/unit pair fails by approximately 1,000-fold; independent X and Y field dimensions establish the reconciled sampling. Maximum field-dimension error 0.00%.

HIGH CONFIDENCE - AUTO-RECONCILED

SIM / Scaling (Per Pixel): 0.021 nm X 0.021 nm X 0.030 nm -> 0.02111 µm X 0.02111 µm X 0.02974 µm. Both numerical magnitude and unit were normalized, then checked against the reported field dimensions; no unit label was changed alone. Supporting evidence: Image Size (Pixels)=1145 X 1654; Image Size (Scaled)=24.17 µm X 34.92 µm; PASS - INTERNALLY CONSISTENT. The source magnitude/unit pair fails by approximately 1,000-fold; independent X and Y field dimensions establish the reconciled sampling. Maximum field-dimension error 0.00%.

HIGH CONFIDENCE - AUTO-RECONCILED

SIM² / Scaling (Per Pixel): 0.021 nm X 0.021 nm X 0.030 nm -> 0.02112 µm X 0.02111 µm X 0.02974 µm. Both numerical magnitude and unit were normalized, then checked against the reported field dimensions; no unit label was changed alone. Supporting evidence: Image Size (Pixels)=250 X 280; Image Size (Scaled)=5.28 µm X 5.91 µm; PASS - INTERNALLY CONSISTENT. The source magnitude/unit pair fails by approximately 1,000-fold; independent X and Y field dimensions establish the reconciled sampling. Maximum field-dimension error 0.00%.

UNRESOLVED - PRESERVED AS CONFLICT

Cross-tier / etoposide duration: Western 20 h; Widefield-SIM2 12 h; STORM 48 h; Control 24 h -> Preserved as modality-specific historical condition values. Twelve hours dominates the conventional-to-SIM2 imaging series, but the record does not establish that Western, STORM and Control used the same preparation. Supporting evidence: The treatment identity and concentration are consistent; duration differs by evidence object.

UNRESOLVED - PRESERVED AS CONFLICT

SIM2 / Image Size (Pixels) Y: 194 pixels with 35.76 µm physical height -> Preserved as conflicting source values. The reported Y pixel count is inconsistent with the physical height and reconciled scale, but the exact intended count cannot be uniquely recovered. Supporting evidence: 0.021 µm/pixel and 35.76 µm imply approximately 1,703 pixels; the source states 194.

UNRESOLVED - PRESERVED AS CONFLICT

SIM / acquisition channel count: Acquisition blocks declare both 3 channels and 2 channels; two laser and excitation entries are present -> Preserved as conflicting source values. The acquisition record does not establish whether the three-channel declaration belongs to a separate image block or is a copied value. Supporting evidence: Laser Wavelength and Excitation Wavelength each contain two entries; the Channels field contains both 3 and 2.

UNRESOLVED - PRESERVED AS CONFLICT

SIM2 / acquisition channel count: Acquisition blocks declare both 3 channels and 2 channels; two laser and excitation entries are present -> Preserved as conflicting source values. The acquisition record does not establish whether the three-channel declaration belongs to a separate image block or is a copied value. Supporting evidence: Laser Wavelength and Excitation Wavelength each contain two entries; the Channels field contains both 3 and 2.

BENNETT

AI-POWERED BIOLOGICAL INTELLIGENCE

BENNETT EVIDENCE REVIEW COMPLETE

INTERPRETATION TO EVIDENCE

BENNETT has completed the bounded retrospective assessment.
The following pages switch ownership to the preserved Identifyn record.

IDENTiFYN®

IDENTIFYN PRESERVED SOURCE EVIDENCE

ORIGINAL RECORD BEGINS

Images, source methods, acquisition settings and provenance follow in the locked Stepdown order. Scientific wording is preserved; missing modalities are not invented.
A preserved control follows all available Stepdown tiers as supporting evidence.

PRODUCT-LEVEL STEPDOWN MAP

This dossier preserves the complete available evidence progression for PA-RR-000013. Each tier remains tied to its original image, source method, instrument context and cryptographic identity. A preserved control is retained as supporting evidence and appears after every resolution tier.

CANONICAL STEPDOWN TIER	EVIDENCE STAGE	INSTRUMENT	STATUS
1	Western blot	Azure Sapphire FL	PRESERVED
2	Widefield	ZEISS Axio Imager.M1	PRESERVED
3	Widefield SIM - Apotome	ZEISS Axio Observer.Z1/7 Apotome	PRESERVED
4	Confocal	ZEISS LSM 980	PRESERVED
5	Airyscan	ZEISS LSM 980	PRESERVED
6	SIM	ZEISS Elyra	PRESERVED
7	SIM²	ZEISS Elyra	PRESERVED
8	Single-molecule STORM	Bruker Vutara VXL	PRESERVED

INTERPRETIVE BOUNDARY

Ordering evidence by resolution tier does not make the modalities interchangeable. Each stage retains its acquisition environment and scientific limitations. This pilot organizes the record; it does not synthesize new biological claims.

ORIGINAL IMAGE EVIDENCE / WESTERN BLOT

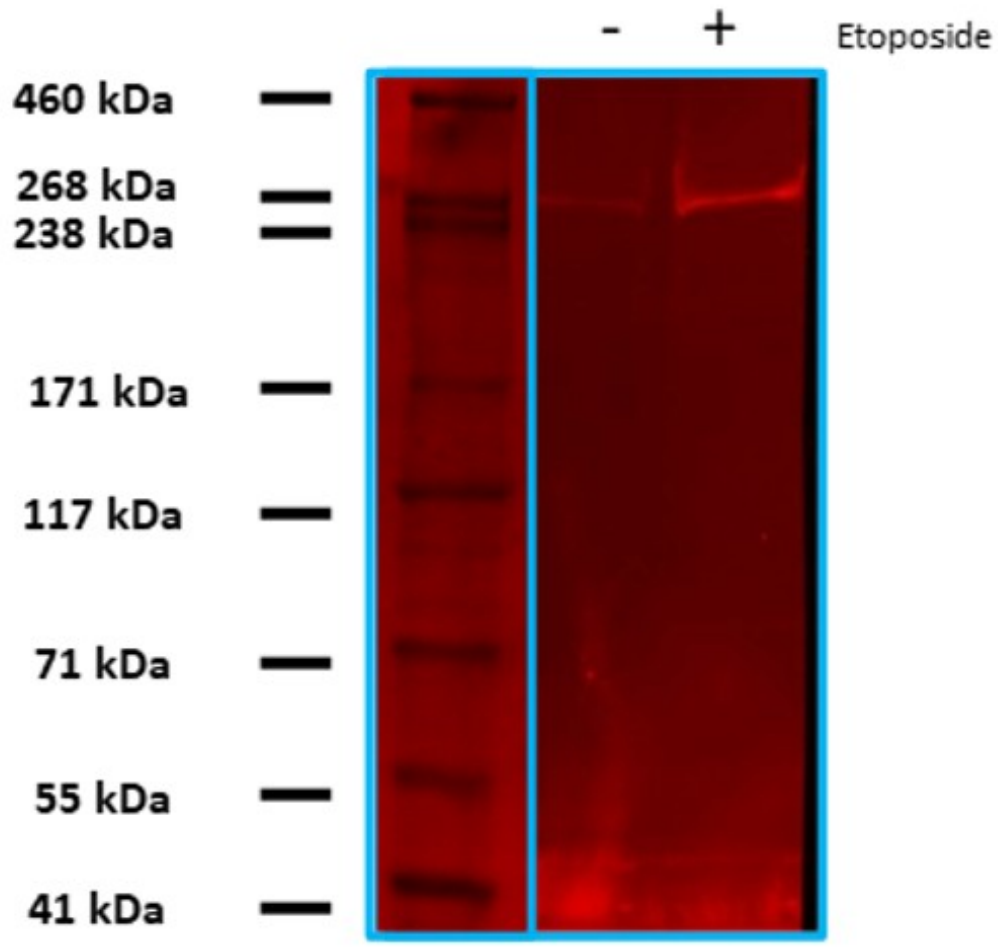

EVIDENCE TIER	Western blot
INSTRUMENT	Azure Sapphire FL
CELL MODEL	HeLa
DETECTED DYES	647
METADATA VALUES	11

STRUCTURED ACQUISITION METADATA / WESTERN BLOT

The values below were deterministically extracted from the preserved Identifyn method PDF text. They remain source-documented metadata, not new BENNETT measurements.

FIELD	SOURCE-DOCUMENTED VALUE
Platform / configuration	Azure Sapphire FL with Customizable Laser and Filter Modules, Enabling UV-NIR and Z-Plane Imaging.
Scanner	Azure Sapphire FL with Customizable Laser and Filter Modules, Enabling UV-NIR and Z-Plane Imaging.
Detection mode	Fluorescence
Laser	638 nm
Emission Filter	676 ± 37 nm
Detector	PMT
Intensity	L3
Pixel size	100 µm
Scan Speed	High
Quality	High
Focus	Membrane (0 µm in Z-axis)
Image	S. Khanal

SOURCE METHOD

The text below is carried from the preserved Identifyn source record. Typography and pagination have been normalized for this preservation dossier; scientific wording has not been editorially rewritten.

Identifyn Standards for Optical Microscopy Methods™

Identifyn® Primary Antibody

Rabbit anti-Human ATR.p (Threonine 1989) Recombinant Monoclonal, IgG - (BLR032P)
Cat ID# - 000013

Expected MW: 301 kDa

HeLa cells were treated with 2 µM etoposide for 20 hours to induce DNA damage. Cells were homogenized using an ultrasonication probe and a nuclear lysis buffer, then centrifuged to pellet the cell debris. The lysate supernatant (100 µg) was mixed with NuPAGE™ LDS Sample Buffer (4X), heated at 80 °C for 10 min, and subjected to electrophoresis on NuPAGE™ Tris-Acetate Mini Protein Gels (3-8%, 1.0 mm) in a Mini Gel Tank. The Thermo Fisher™ HiMark™ Pre-stained Protein Standard was used as a molecular weight marker.

Post electrophoresis, the proteins were transferred to a polyvinylidene difluoride (PVDF) membrane using the iBlot™ 3 Starter Kit PVDF. The transfer membrane was blocked with Blocker™ Casein for 1 hour, then washed 5 times with PBS. The blocked membrane was incubated with Rabbit anti-Human ATR.p (Threonine 1989) Recombinant Monoclonal, IgG - (BLR032P) for 20 hours, followed by 5 washes in 1X PBS. Identifyn® SRM Alexa Fluor™ 647 Affinity Purified Goat Anti-Rabbit IgG (H + L) was incubated for 1 hour and washed 5 times with 1X PBS. The membrane was dried for 10 minutes at room temperature before imaging.

Scanner = Azure Sapphire FL with Customizable Laser and Filter Modules, Enabling UV-NIR and Z-Plane Imaging.

Scan Settings

Detection mode = Fluorescence
Laser = 638 nm
Emission Filter = 676 ± 37 nm
Detector = PMT
Intensity = L3
Pixel size = 100 µm
Scan Speed = High
Quality = High
Focus = Membrane (0 µm in Z-axis)

Post Processing

NONE

Image: S. Khanal

© Copyright 2026 GMD12 LLC.

SOURCE PROVENANCE

Catalog	PA-RR-000013
Stage	Western blot
Instrument	Azure Sapphire FL
Microscope configuration	Azure Sapphire FL with Customizable Laser and Filter Modules, Enabling UV-NIR and Z-Plane Imaging.
Structured source metadata values	11
Metadata source	PRESERVED_SOURCE_METHOD_PDF_TEXT
Cell model	HeLa
Image SHA-256	25182123B02FBB45FDF9BADE235DEA088A975738D50ADEBF321E33BC20582D56
Method PDF SHA-256	A787E61A6AF3C1EEE0E5A3CCB02456285C830860EE45141268F820F92A365E42

ORIGINAL IMAGE EVIDENCE / WIDEFIELD

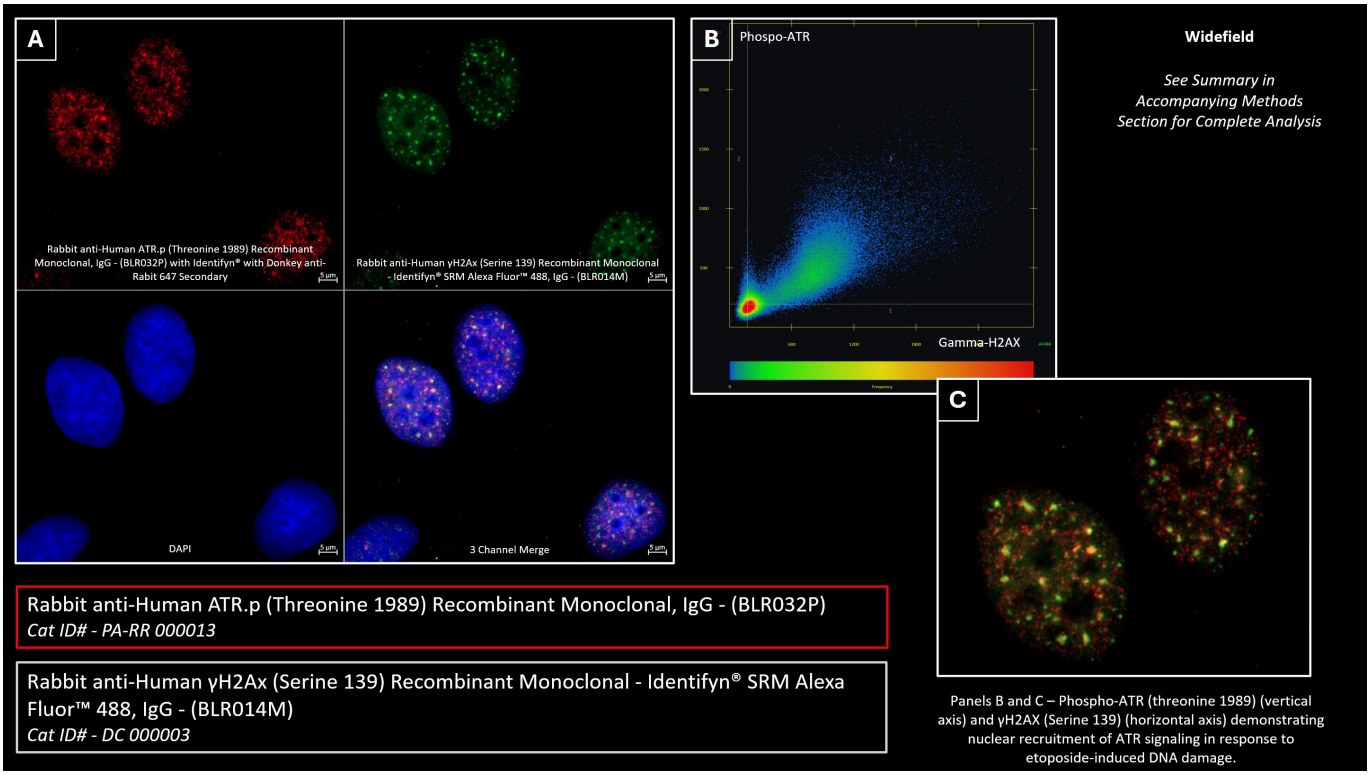

EVIDENCE TIER	Widefield
INSTRUMENT	ZEISS Axio Imager.M1
CELL MODEL	HeLa
DETECTED DYES	405/DAPI; 488; 647
METADATA VALUES	40

STRUCTURED ACQUISITION METADATA / WIDEFIELD

The values below were deterministically extracted from the preserved Identifyn method PDF text. They remain source-documented metadata, not new BENNETT measurements.

FIELD	SOURCE-DOCUMENTED VALUE
Platform / configuration	Zeiss Axio Imager.M1 Widefield, using a Plan-Apochromat 63x/1.40 Oil M27, Axiocam 705, and X-Cite Xylis Lamp, was used with the following parameters for each dye:
Objective	Plan-Apochromat 63x/1.40 Oil M27
Channels	3
Scaling (Per Pixel)	0.110 µm X 0.110 µm
Image Size (Pixels)	834 X 689
Image Size (Scaled)	91.34 µm X 75.46 µm
Bit Depth	14 Bit
Image Center Position	X: 0.00 µm, Y: 0.00 µm
ROI Center Offset	X: 0.00 µm, Y: 0.00 µm
Reflector	50 Cy 5 | 38 eGFP | 49 DAPI
Beam Splitter	660 | 495 | 395
Filter Excitation Wavelength	625 - 655 | 450 - 490 | 335 - 383
Filter Emission Wavelength	665 - 715 | 500 - 550 | 420 - 470
Contrast Method	Fluorescence
Light Source	X-Cite Xylis Lamp Intensity @ 30.00% | X-Cite Xylis Lamp Intensity @ 10.00% | X-Cite Xylis Lamp Intensity @ 5.0%
Exposure Time	300 ms | 100 ms | 15 ms
Excitation Wavelength	653 | 493 | 353
Emission Wavelength	668 | 517 | 465
Effective NA	1.4
Imaging Device	Axiocam 705
Camera Adapter	1X
Depth of Focus	1.03 µm | 0.80 µm | 0.72 µm
Binning Mode	2,2
Image Measurement	Region of Interest from panel A, measuring the two nuclei shown.

SOURCE METHOD

The text below is carried from the preserved Identifyn source record. Typography and pagination have been normalized for this preservation dossier; scientific wording has not been editorially rewritten.

Identifyn Standards for Optical Microscopy Methods™

Identifyn® Primary Antibody

Rabbit anti-Human ATR.p (Threonine 1989) Recombinant Monoclonal, IgG - (BLR032P)
Cat ID# - 000013

Rabbit anti-Human γH2Ax (Serine 139) Recombinant Monoclonal - Identifyn® SRM Alexa Fluor™ 488, IgG - (BLR014M)
Cat ID# - DC 000003

Identifyn® Secondary Antibody

Identifyn® SRM Alexa Fluor™ 647 Affinity Purified Donkey Anti-Rabbit, IgG (H + L)
Cat ID# - SA 000060

ATR (Ataxia Telangiectasia and Rad3-related) is a critical serine/threonine kinase that plays a central role in the cellular response to DNA damage, particularly in response to replication stress and single-strand breaks (SSBs). Unlike ATM (Ataxia Telangiectasia Mutated), which is primarily activated by double-strand breaks, ATR is activated by persistent single-stranded DNA (ssDNA) regions that arise during DNA replication or repair processes.
Overview of ATR Activation

ATR is activated when extensive ssDNA accumulates, often resulting from stalled replication forks or other forms of replication stress. This activation is usually mediated by RPA (Replication Protein A), which binds to ssDNA and recruits ATR and its key activator, ATRIP (ATR Interacting Protein).

Recruitment to Sites of Damage: RPA-coated ssDNA signals DNA damage or replication stress. ATR, with ATRIP, is recruited to these sites, activating ATR's kinase activity.

Interaction with the 9-1-1 Complex: ATR activation is further facilitated by the 9-1-1 complex (comprising RAD9, RAD1, and HUS1), which is loaded onto DNA by RAD17-RFC at sites of DNA damage. This complex interacts with TOPBP1 (Topoisomerase II Binding Protein 1), a key activator of ATR, thereby fully activating ATR kinase activity.

ATR's Role in Single-Strand Break Repair

ATR plays a vital role in facilitating and coordinating the repair of single-strand breaks through various mechanisms:

Checkpoint Activation: ATR is critical for activating checkpoint signaling pathways, notably through phosphorylation of CHK1. This leads to cell cycle arrest or delay, allowing time for DNA repair before cell division continues. This checkpoint activation is crucial in preventing cells from progressing with unrepaired single-strand breaks.

Coordination of Repair Pathways: ATR activation helps coordinate DNA repair processes by recruiting repair proteins and integrating signals across various pathways. This coordination ensures that repair proteins involved in base excision repair (BER), homologous recombination, and other SSB-related pathways are recruited and activated as needed.

Stabilization of Replication Forks: ATR contributes to the stabilization of stalled replication forks, preventing the collapse into double-strand breaks. This is particularly important in preventing the progression of single-strand breaks into more severe DNA damage.

ATR in DNA Damage Response

Beyond its direct role in facilitating single-strand break repair, ATR has broader implications in the DNA damage response:

Genomic Stability: By ensuring proper checkpoint activation and coordinating DNA repair, ATR helps maintain genomic stability, reducing the risk of mutations and chromosomal abnormalities.

Response to Replication Stress: ATR is particularly critical in responding to replication stress, which can result in single-strand breaks due to replication fork stalling or collapse. ATR's activation in these contexts ensures that DNA repair processes are promptly initiated.

ATR is a central player in responding to single-strand breaks and replication stress, activating checkpoint pathways, coordinating DNA repair, and stabilizing replication forks. Through these functions, ATR significantly contributes to maintaining genomic stability and ensuring that cells do not progress with unrepaired DNA damage.

Method

HeLa cells were grown on acid-etched #1.5H cover glass to ~50% confluency. DNA damage was induced by treatment with 2 µM etoposide-spiked complete growth medium for 12 hours, followed by -20 °C methanol fixation and blocking with Thermo Fisher Fish Serum Blocker cat#37527X3. The primary antibody, Rabbit anti-Human ATR.p (Threonine 1989) Recombinant Monoclonal, IgG - (BLR032P), was incubated for 1 hour at room temperature at a dilution of 1:250. Cells were washed 3 times in 1X PBS. Identifyn® SRM Alexa Fluor™ 647 Affinity Purified Donkey Anti-Rabbit, IgG (H + L) was incubated at room temperature for 1 hour at a dilution of 1:1000. Cells were washed 5 times in 1X PBS.

The second primary antibody, Rabbit anti-Human γH2Ax (Serine 139) Recombinant Monoclonal - Identifyn® SRM Alexa Fluor™ 488, IgG - (BLR014M) was incubated for 1 hour at room temperature at a dilution of 1:250. Cells were washed 5 times in 1X PBS and mounted using ProLong™ Diamond Antifade Mountant with DAPI (cat# P36962).

Microscope

Zeiss Axio Imager.M1 Widefield, using a Plan-Apochromat 63x/1.40 Oil M27, Axiocam 705, and X-Cite Xylis Lamp, was used with the following parameters for each dye:

Single Plane (2D)

Channels = 3
Scaling (Per Pixel) = 0.110 µm X 0.110 µm
Image Size (Pixels) = 834 X 689
Image Size (Scaled) = 91.34 µm X 75.46 µm
Bit Depth = 14 Bit
Image Center Position = X: 0.00 µm, Y: 0.00 µm
ROI Center Offset = X: 0.00 µm, Y: 0.00 µm

647 -

Reflector = 50 Cy 5
Beam Splitter = 660
Filter Excitation Wavelength = 625 - 655
Filter Emission Wavelength = 665 - 715
Contrast Method = Fluorescence
Light Source = X-Cite Xylis Lamp Intensity @ 30.00%
Exposure Time = 300 ms
Excitation Wavelength = 653
Emission Wavelength = 668
Effective NA = 1.4
Imaging Device = Axiocam 705
Camera Adapter = 1X
Depth of Focus = 1.03 µm
Binning Mode = 2,2

488 -

Reflector = 38 eGFP
Beam Splitter = 495
Filter Excitation Wavelength = 450 - 490
Filter Emission Wavelength = 500 - 550
Contrast Method = Fluorescence
Light Source = X-Cite Xylis Lamp Intensity @ 10.00%
Exposure Time = 100 ms
Excitation Wavelength = 493
Emission Wavelength = 517
Effective NA = 1.4
Imaging Device = Axiocam 705
Camera Adapter = 1X
Depth of Focus = 0.80 µm
Binning Mode = 2,2

DAPI -

Reflector = 49 DAPI
Beam Splitter = 395
Filter Excitation Wavelength = 335 - 383
Filter Emission Wavelength = 420 - 470
Contrast Method = Fluorescence
Light Source = X-Cite Xylis Lamp Intensity @ 5.0%
Exposure Time = 15 ms
Excitation Wavelength = 353
Emission Wavelength = 465
Effective NA = 1.4
Imaging Device = Axiocam 705
Camera Adapter = 1X
Depth of Focus = 0.72 µm
Binning Mode = 2,2

Split View - Panel A

The top-left panel shows Rabbit anti-Human ATR.p (Threonine 1989) Recombinant Monoclonal, IgG - (BLR032P), visualized using Identifyn® SRM Alexa Fluor™ 647 Affinity Purified Donkey Anti-Rabbit, IgG (H + L) secondary antibody. The top-right panel shows Rabbit anti-Human γH2Ax (Serine 139) Recombinant Monoclonal - Identifyn® SRM Alexa Fluor™ 488, IgG - (BLR014M). The lower-left panel shows DAPI staining, and the bottom-right panel shows the three-channel merged image.

Colocalization View - Panels B and C

Vertical Axis - AF647, Threshold 196, Range Auto
Horizontal Axis - AF488, Threshold 174, Range Auto

Image Measurement = Region of Interest from panel A, measuring the two nuclei shown.

Colocalization analysis between phospho-ATR (Threonine 1989) and γH2AX (Serine 139) (Alexa Fluor 488 direct conjugate) was conducted using a defined ROI containing two nuclei from Panel A. The analysis demonstrates strong spatial colocalization between phospho-ATR and γH2AX foci, supporting ATR activation and localization at DNA damage sites within the nucleus.

Summary

Shows Rabbit anti-Human ATR.p (Threonine 1989) Recombinant Monoclonal, IgG - (BLR032P), visualized using Identifyn® SRM Alexa Fluor™ 647 Affinity Purified Donkey Anti-Rabbit, IgG (H + L), alongside Rabbit anti-Human γH2Ax (Serine 139) Recombinant Monoclonal - Identifyn® SRM Alexa Fluor™ 488, IgG - (BLR014M), and DAPI nuclear counterstaining. Under widefield fluorescence microscopy conditions, strong nuclear-associated ATR.p signal and discrete γH2Ax-associated DNA damage foci were observed following etoposide-induced replication stress, supporting robust target-specific staining and biologically consistent ATR activation patterns. Apparent colocalization between ATR.p and γH2Ax foci was observed throughout damaged nuclei; however, due to the diffraction-limited resolution of widefield microscopy, the precise nanoscale spatial relationship between ATR.p signaling domains and γH2Ax-associated chromatin structures cannot be definitively resolved at this imaging stage. This dataset therefore serves as the initial step in the Identifyn™ Stepdown Methodology™, establishing biologically consistent damage-associated signal overlap prior to higher-resolution evaluation using confocal, Airyscan, Lattice SIM, SIM², and STORM imaging workflows.

Image Correction

NONE

Image by E.F.Simon
Image Analysis and Data Presentation by B.T. Bennett

© Copyright 2026 GMD12 LLC.

SOURCE PROVENANCE

Catalog	PA-RR-000013
Stage	Widefield
Instrument	ZEISS Axio Imager.M1

SOURCE PROVENANCE

Microscope configuration	Zeiss Axio Imager.M1 Widefield, using a Plan-Apochromat 63x/1.40 Oil M27, Axiocam 705, and X-Cite Xylis Lamp, was used with the following parame
Structured source metadata values	40
Metadata source	PRESERVED_SOURCE_METHOD_PDF_TEXT
Cell model	HeLa
Image SHA-256	3CF07153B3EE72602DFFA8A08D25883D5C58BBF22500A6CB8C2A171BCAE45E62
Method PDF SHA-256	E4A4C9165FF7779559DA353AAAFE3E093FE7233A0C611C71CB508D496D05AB5B

ORIGINAL IMAGE EVIDENCE / WIDEFIELD SIM - APOTOME

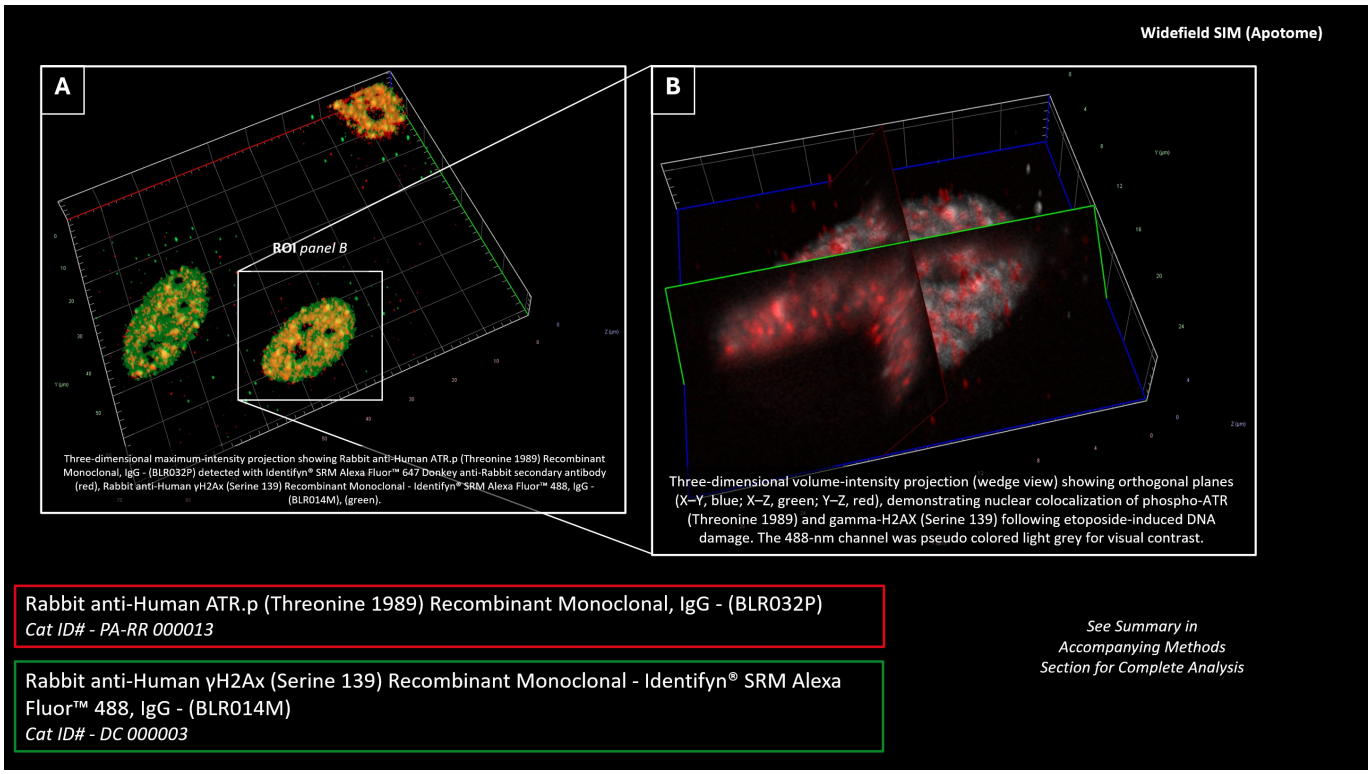

EVIDENCE TIER	Widefield SIM - Apotome
INSTRUMENT	ZEISS Axio Observer.Z1/7 Apotome
CELL MODEL	HeLa
DETECTED DYES	405/DAPI; 488; 647
METADATA VALUES	65

STRUCTURED ACQUISITION METADATA / WIDEFIELD SIM - APOTOME

The values below were deterministically extracted from the preserved Identifyn method PDF text. They remain source-documented metadata, not new BENNETT measurements.

FIELD	SOURCE-DOCUMENTED VALUE
Platform / configuration	Zeiss Axio Observer.Z1/7 Apotome SIM, using an EC Plan-Neofluar 63X/1.25 oil M27, Axiocam 807 Mono, and X-Cite Xylis Lamp was used with the following parameters for each dye:
Objective	EC Plan-Neofluar 63X/1.25 oil M27
Z-Stack	85 Slices (8.4 µm) | 47 Slices (4.6 µm), Z-stack was trimmed via the Gallery Tool, to remove non-data-bearing Z-planes
Channels	3
Scaling (Per Pixel)	0.143 µm X 0.143 µm X 0.100 µm
Image Size (Pixels)	621 X 500 | 217 X 173
Image Size (Scaled)	88.71 µm X 71.43 µm | 31.00 µm X 24.71 µm
Bit Depth	14 Bit
Image Center Position	X: 46.89 mm, Y: 50.53 mm
Stage Position	X: 46.89 mm, Y: 50.53 mm
ROI Center Offset	X: 1.14 µm, Y: 0.00 µm
Reflector	50 Cy 5 | 38 eGFP | 49 DAPI
Beam Splitter	660 | 495 | 395
Filter Excitation Wavelength	625 - 655 | 450 - 490 | 335 - 383
Filter Emission Wavelength	665 - 715 | 500 - 550 | 420 - 470
Contrast Method	Fluorescence
Light Source	X-Cite Xylis Lamp Intensity @ 25.00% | X-Cite Xylis Lamp Intensity @ 10.00% | X-Cite Xylis Lamp Intensity @ 5.00%
Exposure Time	250 ms | 100 ms | 15 ms
Excitation Wavelength	653 | 493 | 353
Emission Wavelength	668 | 517 | 465
Effective NA	1.25 | 1.4
Imaging Device	Axiocam 807 Mono
Camera Adapter	1X
Depth of Focus	1.30 µm | 1.00 µm | 0.72 µm
Binning Mode	2,2
Apotome SIM Image Processing	Display Mode "Optical Sectioning" - enabled correction selected.
3D Maximum Projection	Precise
Appearance	Threshold 13% all channels, Ramp 0% all channels, Maximum 100% all channels | Threshold 13% all channels, Ramp 50% all channels, Maximum 100% all channels
Background	Black
Light	Brightness 90%, Enabled Tone Mapping | Brightness 100%, Azimuth 80°, Elongation -130°, Enabled Directional Lighting, Enabled Tone Mapping

FIELD	SOURCE-DOCUMENTED VALUE
Projection	View Angle 35°, Scale Z 50%, Reverse Z-Axis NOT Selected, Stereo Anaglyph NOT Selected, Camera Separation 5% (deselected), Parallax Shift 0% (deselected) | View Angle 35°, Scale Z 100%, Reverse Z-Axis NOT Selected, Stereo Anaglyph NOT Selected, Camera Separation 5% (deselected), Parallax Shift 0% (deselected)
3D Volume Projection	Precise
X-Y	Activate was selected, textured opaque was chosen, and a blue outline of the clipped perimeter was shown; Clip Back was selected, and Clip Front was NOT selected.
Position of Clip	-93% | 13% | 3%
Clip X	0°
Clip Z	0°
X-Z	Activate was selected, textured opaque was chosen, and a green outline of the clipped perimeter was shown; Clip Back was selected, and Clip Front was NOT selected.
Clip Y	45° | -45°
Y-Z	Activate was selected, textured opaque was chosen, and a red outline of the clipped perimeter was shown; Clip Back was selected, and Clip Front was NOT selected.

SOURCE METHOD

The text below is carried from the preserved Identifyn source record. Typography and pagination have been normalized for this preservation dossier; scientific wording has not been editorially rewritten.

Identifyn Standards for Optical Microscopy Methods™

Identifyn® Primary Antibody

Rabbit anti-Human ATR.p (Threonine 1989) Recombinant Monoclonal, IgG - (BLR032P)
Cat ID# - 000013

Rabbit anti-Human γH2Ax (Serine 139) Recombinant Monoclonal - Identifyn® SRM Alexa Fluor™ 488, IgG - (BLR014M)
Cat ID# - DC 000003

Identifyn® Secondary Antibody

Identifyn® SRM Alexa Fluor™ 647 Affinity Purified Donkey Anti-Rabbit, IgG (H + L)
Cat ID# - SA 000060

ATR (Ataxia Telangiectasia and Rad3-related) is a critical serine/threonine kinase that plays a central role in the cellular response to DNA damage, particularly in response to replication stress and single-strand breaks (SSBs). Unlike ATM (Ataxia Telangiectasia Mutated), which is primarily activated by double-strand breaks, ATR is activated by persistent single-stranded DNA (ssDNA) regions that arise during DNA replication or repair processes.
Overview of ATR Activation

ATR is activated when extensive ssDNA accumulates, often resulting from stalled replication forks or other forms of replication stress. This activation is usually mediated by RPA (Replication Protein A), which binds to ssDNA and recruits ATR and its key activator, ATRIP (ATR Interacting Protein).

Recruitment to Sites of Damage: RPA-coated ssDNA signals DNA damage or replication stress. ATR, with ATRIP, is recruited to these sites, activating ATR's kinase activity.

Interaction with the 9-1-1 Complex: ATR activation is further facilitated by the 9-1-1 complex (comprising RAD9, RAD1, and HUS1), which is loaded onto DNA by RAD17-RFC at sites of DNA damage. This complex interacts with TOPBP1 (Topoisomerase II Binding Protein 1), a key activator of ATR, thereby fully activating ATR kinase activity.

ATR's Role in Single-Strand Break Repair

ATR plays a vital role in facilitating and coordinating the repair of single-strand breaks through various mechanisms:

Checkpoint Activation: ATR is critical for activating checkpoint signaling pathways, notably through phosphorylation of CHK1. This leads to cell cycle arrest or delay, allowing time for DNA repair before cell division continues. This checkpoint activation is crucial in preventing cells from progressing with unrepaired single-strand breaks.

Coordination of Repair Pathways: ATR activation helps coordinate DNA repair processes by recruiting repair proteins and integrating signals across various pathways. This coordination ensures that repair proteins involved in base excision repair (BER), homologous recombination, and other SSB-related pathways are recruited and activated as needed.

Stabilization of Replication Forks: ATR contributes to the stabilization of stalled replication forks, preventing the collapse into double-strand breaks. This is particularly important in preventing the progression of single-strand breaks into more severe DNA damage.

ATR in DNA Damage Response

Beyond its direct role in facilitating single-strand break repair, ATR has broader implications in the DNA damage response:

Genomic Stability: By ensuring proper checkpoint activation and coordinating DNA repair, ATR helps maintain genomic stability, reducing the risk of mutations and chromosomal abnormalities.

Response to Replication Stress: ATR is particularly critical in responding to replication stress, which can result in single-strand breaks due to replication fork stalling or collapse. ATR's activation in these contexts ensures that DNA repair processes are promptly initiated.

ATR is a central player in responding to single-strand breaks and replication stress, activating checkpoint pathways, coordinating DNA repair, and stabilizing replication forks. Through these functions, ATR significantly contributes to maintaining genomic stability and ensuring that cells do not progress with unrepaired DNA damage.

Method

HeLa cells were grown on acid-etched #1.5H cover glass to ~50% confluency. DNA damage was induced by treatment with 2 µM etoposide-spiked complete growth medium for 12 hours, followed by -20 °C methanol fixation and blocking with Thermo Fisher Fish Serum Blocker cat#37527X3. The primary antibody, Rabbit anti-Human ATR.p (Threonine 1989) Recombinant Monoclonal, IgG - (BLR032P), was incubated for 1 hour at room temperature at a dilution of 1:250. Cells were washed 3 times in 1X PBS. Identifyn® SRM Alexa Fluor™ 647 Affinity Purified Donkey Anti-Rabbit, IgG (H + L) was incubated at room temperature for 1 hour at a dilution of 1:1000. Cells were washed 5 times in 1X PBS.

The second primary antibody, Rabbit anti-Human γH2Ax (Serine 139) Recombinant Monoclonal - Identifyn® SRM Alexa Fluor™ 488, IgG - (BLR014M) was incubated for 1 hour at room temperature at a dilution of 1:250. Cells were washed 5 times in 1X PBS and mounted using ProLong™ Diamond Antifade Mountant with DAPI (cat# P36962).

Microscope

Zeiss Axio Observer.Z1/7 Apotome SIM, using an EC Plan-Neofluar 63X/1.25 oil M27, Axiocam 807 Mono, and X-Cite Xylis Lamp was used with the following parameters for each dye:

Z Stack - (3D) - Panel A

Z-Stack = 85 Slices (8.4 µm)

Channels = 3
Scaling (Per Pixel) = 0.143 µm X 0.143 µm X 0.100 µm
Image Size (Pixels) = 621 X 500
Image Size (Scaled) = 88.71 µm X 71.43 µm
Bit Depth = 14 Bit
Image Center Position = X: 46.89 mm, Y: 50.53 mm
Stage Position = X: 46.89 mm, Y: 50.53 mm
ROI Center Offset = X: 1.14 µm, Y: 0.00 µm

Z Stack - (3D) - Panel B, Region of Interest

Z-Stack = 47 Slices (4.6 µm), Z-stack was trimmed via the Gallery Tool, to remove non-data-bearing Z-planes

Channels = 3
Scaling (Per Pixel) = 0.143 µm X 0.143 µm X 0.100 µm
Image Size (Pixels) = 217 X 173
Image Size (Scaled) = 31.00 µm X 24.71 µm

Bit Depth = 14 Bit
Image Center Position = X: 46.89 mm, Y: 50.53 mm
Stage Position = X: 46.89 mm, Y: 50.53 mm
ROI Center Offset = X: 1.14 µm, Y: 0.00 µm

647 -

Reflector = 50 Cy 5
Beam Splitter = 660
Filter Excitation Wavelength = 625 - 655
Filter Emission Wavelength = 665 - 715
Contrast Method = Fluorescence
Light Source = X-Cite Xylis Lamp Intensity @ 25.00%
Exposure Time = 250 ms
Excitation Wavelength = 653
Emission Wavelength = 668
Effective NA = 1.25
Imaging Device = Axiocam 807 Mono
Camera Adapter = 1X
Depth of Focus = 1.30 µm
Binning Mode = 2,2

488 -

Reflector = 38 eGFP
Beam Splitter = 495
Filter Excitation Wavelength = 450 - 490
Filter Emission Wavelength = 500 - 550
Contrast Method = Fluorescence
Light Source = X-Cite Xylis Lamp Intensity @ 10.00%
Exposure Time = 100 ms
Excitation Wavelength = 493
Emission Wavelength = 517
Effective NA = 1.25
Imaging Device = Axiocam 807 Mono
Camera Adapter = 1X
Depth of Focus = 1.00 µm
Binning Mode = 2,2

DAPI - Collected but not Shown in Data Representation

Reflector = 49 DAPI
Beam Splitter = 395
Filter Excitation Wavelength = 335 - 383
Filter Emission Wavelength = 420 - 470
Contrast Method = Fluorescence
Light Source = X-Cite Xylis Lamp Intensity @ 5.00%
Exposure Time = 15 ms
Excitation Wavelength = 353
Emission Wavelength = 465
Effective NA = 1.4
Imaging Device = Axiocam 807 Mono
Camera Adapter = 1X
Depth of Focus = 0.72 µm
Binning Mode = 2,2

Post Processing - SIM Processing

Apotome SIM Image Processing = Display Mode "Optical Sectioning" - enabled correction selected. Normalization, Phase Corrector, Fourier Filter, and Deconvolution were NOT used.

3D Image Processing - Panel A

3D Maximum Projection = Precise
Appearance = Threshold 13% all channels, Ramp 0% all channels, Maximum 100% all channels
Background = Black
Light = Brightness 90%, Enabled Tone Mapping
Projection = View Angle 35°, Scale Z 50%, Reverse Z-Axis NOT Selected, Stereo Anaglyph NOT Selected, Camera Separation 5% (deselected), Parallax Shift 0% (deselected)

3D Image Processing - Panel B

3D Volume Projection = Precise
Appearance = Threshold 13% all channels, Ramp 50% all channels, Maximum 100% all channels
Background = Black
Light = Brightness 100%, Azimuth 80°, Elongation -130°, Enabled Directional Lighting, Enabled Tone Mapping
Projection = View Angle 35°, Scale Z 100%, Reverse Z-Axis NOT Selected, Stereo Anaglyph NOT Selected, Camera Separation 5% (deselected), Parallax Shift 0% (deselected)

Clipping Image Process - Panel B

Clipping planes are introduced in Panel B to highlight the nuclear colocalization of the phospho-ATR with gamma-H2AX in response to etoposide-induced DNA damage within the nuclear compartment by adjusting or cutting away portions of the image using a triple-wedge cut, removing parts of the image in the X-Y, X-Z, and Y-Z planes.

X-Y = Activate was selected, textured opaque was chosen, and a blue outline of the clipped perimeter was shown; Clip Back was selected, and Clip Front was NOT selected.

Position of Clip = -93%
Clip X = 0°
Clip Z = 0°

X-Z = Activate was selected, textured opaque was chosen, and a green outline of the clipped perimeter was shown; Clip Back was selected, and Clip Front was NOT selected.

Position of Clip = 13%
Clip Y = 45°
Clip Z = 0°

Y-Z = Activate was selected, textured opaque was chosen, and a red outline of the clipped perimeter was shown; Clip Back was selected, and Clip Front was NOT selected.

Position of Clip = 3%
Clip Y = -45°
Clip Z = 0°

Panel B shows a wedge-cut view displayed from the top with a slight backward rotation, highlighting the region of wedge removal and revealing the full depth of signal across the z-stack. This orientation provides an alternative view of wedge geometry and confirms nuclear colocalization of the phospho-ATR and gamma-H2AX in response to etoposide-induced DNA damage within the nuclear compartment.

Summary

Panel A presents a three-dimensional Apotome SIM acquisition following etoposide-induced DNA damage, showing Rabbit anti-Human ATR.p (Threonine 1989) Recombinant Monoclonal, IgG - (BLR032P), visualized using Identifyn® SRM Alexa Fluor™ 647 Affinity Purified Donkey Anti-Rabbit, IgG (H + L), together with Rabbit anti-Human γH2Ax (Serine 139) Recombinant Monoclonal - Identifyn® SRM Alexa Fluor™ 488, IgG - (BLR014M). Compared with conventional widefield imaging, Apotome SIM optical sectioning improves axial discrimination and reduces out-of-focus fluorescence, enabling enhanced visualization of ATR.p-associated DNA damage response territories within the nuclear volume. Following etoposide exposure, ATR.p exhibited pronounced intranuclear redistribution and punctate damage-associated signaling structures that overlapped with γH2Ax-enriched nuclear regions, consistent with coordinated replication stress and DNA damage checkpoint activation.

Panel B presents a wedge-cut volumetric reconstruction of the same dataset using orthogonal clipping planes to interrogate signal distribution throughout the z-stack. The clipping workflow reveals that ATR.p and γH2Ax signals occupy shared nuclear response territories across multiple focal planes, while simultaneously illustrating the limitations of diffraction-limited optical sectioning approaches. Although Apotome SIM improves volumetric interpretation compared with standard widefield microscopy, individual DNA damage foci, repair subdomains, and nanoscale signaling architectures remain unresolved at this imaging stage. Thus, the observed overlap should be interpreted as biologically coordinated recruitment within DNA damage-associated nuclear territories rather than definitive molecular colocalization.

Importantly, this dataset represents a critical transitional stage within the Identifyn® Stepdown Methodology™, bridging diffraction-limited widefield imaging and higher-resolution confocal and super-resolution modalities. The progression from widefield to Apotome SIM demonstrates how improved optical sectioning progressively refines apparent signal overlap while preserving biologically coherent ATR.p and γH2Ax-associated DNA damage response behavior prior to higher-resolution interrogation by confocal, Airyscan, Lattice SIM, SIM², and STORM imaging workflows.

Image Correction

NONE

Image by E.F.Simon
Image Analysis and Data Presentation by B.T. Bennett

© Copyright 2026 GMD12 LLC.

SOURCE PROVENANCE

Catalog	PA-RR-000013
Stage	Widefield SIM - Apotome
Instrument	ZEISS Axio Observer.Z1/7 Apotome
Microscope configuration	Zeiss Axio Observer.Z1/7 Apotome SIM, using an EC Plan-Neofluar 63X/1.25 oil M27, Axiocam 807 Mono, and X-Cite Xylis Lamp was used with the fol
Structured source metadata values	65
Metadata source	PRESERVED_SOURCE_METHOD_PDF_TEXT
Cell model	HeLa
Image SHA-256	0A27FC451A47C60B03C1044F9F1BD30C6423556F58245424FB3C6F9F2876E12D
Method PDF SHA-256	9FA543F24FCCBA0839F79499AFD3254A57824DCD642B7CEB94437541C8333BFE

ORIGINAL IMAGE EVIDENCE / CONFOCAL

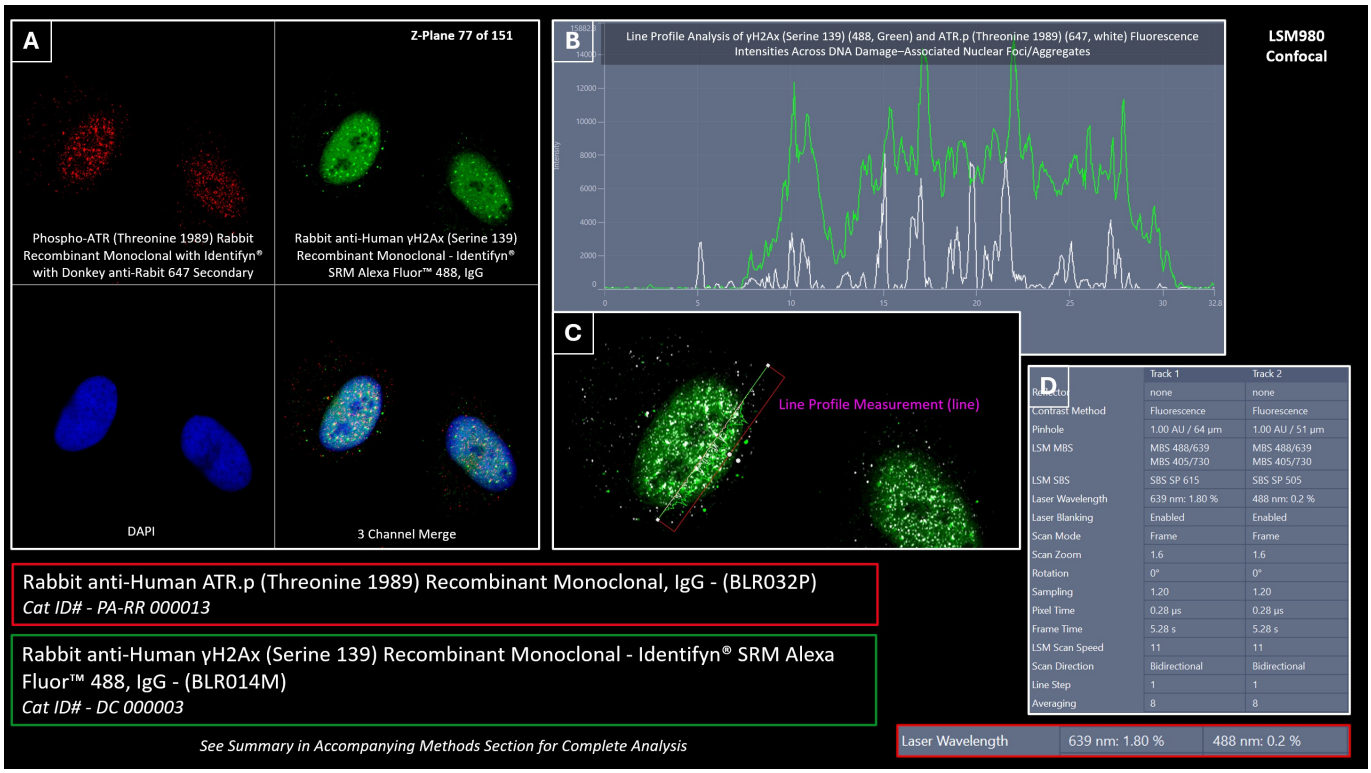

EVIDENCE TIER	Confocal
INSTRUMENT	ZEISS LSM 980
CELL MODEL	HeLa
DETECTED DYES	405/DAPI; 488; 647
METADATA VALUES	53

STRUCTURED ACQUISITION METADATA / CONFOCAL

The values below were deterministically extracted from the preserved Identifyn method PDF text. They remain source-documented metadata, not new BENNETT measurements.

FIELD	SOURCE-DOCUMENTED VALUE
Platform / configuration	Zeiss LSM980 Confocal with NIR Detection, Axio Observer.Z1/7, using a Plan-Apochromat 63x/1.40 Oil DIC M27, was used with the following parameters for each dye:
Objective	Plan-Apochromat 63x/1.40 Oil DIC M27
Z-Stack	151 Slices (4.5 µm)
Channels	3
Scaling (Per Pixel)	0.059 µm X 0.059 µm X 0.030 µm
Image Size (Pixels)	1407 X 1407
Image Size (Scaled)	82.77 µm X 82.77 µm
Bit Depth	16 Bit
Image Center Position	X: 91.51 mm, Y: 49.99 mm
Stage Position	X: 91.51 mm, Y: 49.99 mm
ROI Center Offset	X: 0.00 µm, Y: 0.00 µm
Reflector	None
Contrast Method	Fluorescence
Pinhole	1.00 AU / 64 µm | 1.00 AU / 51 µm | 1.00 AU / 43 µm
LMS MBS	MBS 488/639 & 405/730
LMS SBS	SBS SP 615 | SBS SP 505 | Mirror
Laser Wavelength	639 nm @ 1.8% | 488 nm @ 0.2% | 405 nm @ 0.2%
Laser Blanking	Enabled
Scan Mode	Frame
Scan Zoom	1.6
Rotation	0°
Sampling	1.20
Pixel Time	0.28 µs
Frame Time	5.28 s
LSM Scan Speed	11
Scan Direction	Bidirectional
Line Step	1
Averaging	8
Excitation Wavelength	653 | 493 | 353
Emission Wavelength	668 | 517 | 465
Effective NA	1.4
Detection Wavelength	647 - 700 | 511 - 550 | 435 - 470
Imaging Device	GaAsP-Pmt3

FIELD	SOURCE-DOCUMENTED VALUE
Detector Type	GaAsP-PMT
Detector Gain	550 V | 500 V
Detector Offset	0
Detector Digital Gain	1.0
LSM Plus Mode	Filter: 8.6 (3D, Auto) | Filter: 7.2 (3D, Auto) | Filter: 6.8 (3D, Auto)
Profile Definition	Stroke Thickness 1, Normal View, Grid Distance 1
Profile View	X and Y axes were set to Auto - X (Min 0.0 and Max 32.8), Y (Min 0 and Max 14594)

SOURCE METHOD

The text below is carried from the preserved Identifyn source record. Typography and pagination have been normalized for this preservation dossier; scientific wording has not been editorially rewritten.

Identifyn Standards for Optical Microscopy Methods™

Identifyn® Primary Antibody

Rabbit anti-Human ATR.p (Threonine 1989) Recombinant Monoclonal, IgG - (BLR032P)
Cat ID# - 000013

Rabbit anti-Human γH2Ax (Serine 139) Recombinant Monoclonal - Identifyn® SRM Alexa Fluor™ 488, IgG - (BLR014M)
Cat ID# - DC 000003

Identifyn® Secondary Antibody

Identifyn® SRM Alexa Fluor™ 647 Affinity Purified Donkey Anti-Rabbit, IgG (H + L)
Cat ID# - SA 000060

ATR (Ataxia Telangiectasia and Rad3-related) is a critical serine/threonine kinase that plays a central role in the cellular response to DNA damage, particularly in response to replication stress and single-strand breaks (SSBs). Unlike ATM (Ataxia Telangiectasia Mutated), which is primarily activated by double-strand breaks, ATR is activated by persistent single-stranded DNA (ssDNA) regions that arise during DNA replication or repair processes.
Overview of ATR Activation

ATR is activated when extensive ssDNA accumulates, often resulting from stalled replication forks or other forms of replication stress. This activation is usually mediated by RPA (Replication Protein A), which binds to ssDNA and recruits ATR and its key activator, ATRIP (ATR Interacting Protein).

Recruitment to Sites of Damage: RPA-coated ssDNA signals DNA damage or replication stress. ATR, with ATRIP, is recruited to these sites, activating ATR's kinase activity.

Interaction with the 9-1-1 Complex: ATR activation is further facilitated by the 9-1-1 complex (comprising RAD9, RAD1, and HUS1), which is loaded onto DNA by RAD17-RFC at sites of DNA damage. This complex interacts with TOPBP1 (Topoisomerase II Binding Protein 1), a key activator of ATR, thereby fully activating ATR kinase activity.

ATR's Role in Single-Strand Break Repair

ATR plays a vital role in facilitating and coordinating the repair of single-strand breaks through various mechanisms:

Checkpoint Activation: ATR is critical for activating checkpoint signaling pathways, notably by phosphorylating CHK1. This leads to cell cycle arrest or delay, allowing time for DNA repair before cell division continues. This checkpoint activation is crucial in preventing cells from progressing with unrepaired single-strand breaks.

Coordination of Repair Pathways: ATR activation helps coordinate DNA repair processes by recruiting repair proteins and integrating signals across various pathways. This coordination ensures that repair proteins involved in base excision repair (BER), homologous recombination, and other SSB-related pathways are recruited and activated as needed.

Stabilization of Replication Forks: ATR contributes to the stabilization of stalled replication forks, preventing the collapse into double-strand breaks. This is particularly important in preventing the progression of single-strand breaks into more severe DNA damage.

ATR in DNA Damage Response

Beyond its direct role in facilitating single-strand break repair, ATR has broader implications in the DNA damage response:

Genomic Stability: By ensuring proper checkpoint activation and coordinating DNA repair, ATR helps maintain genomic stability, reducing the risk of mutations and chromosomal abnormalities.

Response to Replication Stress: ATR is particularly critical in responding to replication stress, which can result in single-strand breaks due to replication fork stalling or collapse. ATR's activation in these contexts ensures that DNA repair processes are promptly initiated.

ATR is a central player in responding to single-strand breaks and replication stress, activating checkpoint pathways, coordinating DNA repair, and stabilizing replication forks. Through these functions, ATR significantly contributes to maintaining genomic stability and ensuring that cells do not progress with unrepaired DNA damage.

Method

HeLa cells were grown on acid-etched #1.5H cover glass to ~50% confluency. DNA damage was induced by treatment with 2 µM etoposide-spiked complete growth medium for 12 hours, followed by -20 °C methanol fixation and blocking with Thermo Fisher Fish Serum Blocker cat#37527X3. The primary antibody, Rabbit anti-Human ATR.p (Threonine 1989) Recombinant Monoclonal, IgG - (BLR032P), was incubated for 1 hour at room temperature at a dilution of 1:250. Cells were washed 3 times in 1X PBS. Identifyn® SRM Alexa Fluor™ 647 Affinity Purified Donkey Anti-Rabbit, IgG (H + L) was incubated at room temperature for 1 hour at a dilution of 1:1000. Cells were washed 5 times in 1X PBS.

The second primary antibody, Rabbit anti-Human γH2Ax (Serine 139) Recombinant Monoclonal - Identifyn® SRM Alexa Fluor™ 488, IgG - (BLR014M) was incubated for 1 hour at room temperature at a dilution of 1:250. Cells were washed 5 times in 1X PBS and mounted using ProLong™ Diamond Antifade Mountant with DAPI (cat# P36962).

Microscope

Zeiss LSM980 Confocal with NIR Detection, Axio Observer.Z1/7, using a Plan-Apochromat 63x/1.40 Oil DIC M27, was used with the following parameters for each dye:

Z Stack - (3D) - 2D at Z-Plane 77 of 151, Panels A, B, and C

Z-Stack = 151 Slices (4.5 µm)

Channels = 3
Scaling (Per Pixel) = 0.059 µm X 0.059 µm X 0.030 µm
Image Size (Pixels) = 1407 X 1407
Image Size (Scaled) = 82.77 µm X 82.77 µm
Bit Depth = 16 Bit
Image Center Position = X: 91.51 mm, Y: 49.99 mm
Stage Position = X: 91.51 mm, Y: 49.99 mm
ROI Center Offset = X: 0.00 µm, Y: 0.00 µm

647 -

Reflector = None
Contrast Method = Fluorescence
Pinhole = 1.00 AU / 64 µm
LMS MBS = MBS 488/639 & 405/730
LMS SBS = SBS SP 615
Laser Wavelength = 639 nm @ 1.8%
Laser Blanking = Enabled
Scan Mode = Frame
Scan Zoom = 1.6
Rotation = 0°
Sampling = 1.20
Pixel Time = 0.28 µs
Frame Time = 5.28 s
LSM Scan Speed = 11
Scan Direction = Bidirectional
Line Step = 1
Averaging = 8
Excitation Wavelength = 653
Emission Wavelength = 668
Effective NA = 1.4
Detection Wavelength = 647 - 700
Imaging Device = GaAsP-Pmt3
Detector Type = GaAsP-PMT
Detector Gain = 550 V
Detector Offset = 0
Detector Digital Gain = 1.0
LSM Plus Mode = Filter: 8.6 (3D, Auto)

488 -

Reflector = None
Contrast Method = Fluorescence
Pinhole = 1.00 AU / 51 µm
LMS MBS = MBS 488/639 & 405/730
LMS SBS = SBS SP 505
Laser Wavelength = 488 nm @ 0.2%
Laser Blanking = Enabled
Scan Mode = Frame
Scan Zoom = 1.6
Rotation = 0°
Sampling = 1.20
Pixel Time = 0.28 µs
Frame Time = 5.28 s
LSM Scan Speed = 11
Scan Direction = Bidirectional
Line Step = 1
Averaging = 8
Excitation Wavelength = 493
Emission Wavelength = 517
Effective NA = 1.4
Detection Wavelength = 511 - 550
Imaging Device = GaAsP-Pmt3
Detector Type = GaAsP-PMT
Detector Gain = 500 V
Detector Offset = 0
Detector Digital Gain = 1.0
LSM Plus Mode = Filter: 7.2 (3D, Auto)

DAPI -

Reflector = None
Contrast Method = Fluorescence
Pinhole = 1.00 AU / 43 µm
LMS MBS = MBS 488/639 & 405/730
LMS SBS = Mirror
Laser Wavelength = 405 nm @ 0.2%
Laser Blanking = Enabled
Scan Mode = Frame
Scan Zoom = 1.6
Rotation = 0°
Sampling = 1.20
Pixel Time = 0.28 µs
Frame Time = 5.28 s
LSM Scan Speed = 11
Scan Direction = Bidirectional
Line Step = 1
Averaging = 8
Excitation Wavelength = 353
Emission Wavelength = 465
Effective NA = 1.4
Detection Wavelength = 435 - 470
Imaging Device = GaAsP-Pmt3
Detector Type = GaAsP-PMT
Detector Gain = 500 V
Detector Offset = 0
Detector Digital Gain = 1.0
LSM Plus Mode = Filter: 6.8 (3D, Auto)

Split View - Panel A

The top-left panel shows Rabbit anti-Human ATR.p (Threonine 1989) Recombinant Monoclonal, IgG - (BLR032P), visualized using Identifyn® SRM Alexa Fluor™ 647 Affinity Purified Donkey Anti-Rabbit, IgG (H + L) secondary antibody. The top-right panel shows Rabbit anti-Human γH2Ax (Serine 139) Recombinant Monoclonal - Identifyn® SRM Alexa Fluor™ 488, IgG - (BLR014M). The lower-left panel shows DAPI staining, and the bottom-right panel shows the three-channel merged image.

Profile View Display - Panels B & C

Profile Definition = Stroke Thickness 1, Normal View, Grid Distance 1
Profile View = X and Y axes were set to Auto - X (Min 0.0 and Max 32.8), Y (Min 0 and Max 14594)

This panel quantifies colocalized foci, or resolution-limited aggregates, of phospho-ATR and γH2AX following etoposide-induced DNA damage. Line profile analysis reveals strong spatial concordance and comparable signal intensity distributions, supporting strong coordinated recruitment and overlapping damage-associated signaling territories.

Zen Acquisition Info Tab - Panel D

Shown are the acquisition parameters for the 647 channel (phospho-ATR) and 488 channel (γH2AX), collected using the 639 nm laser at 1.8% power and the 488 nm laser at 0.2% power, respectively. Scan zoom, scan speed, and line-averaging settings are provided to ensure the transparency and reproducibility of line-profile measurements.

Summary

Panel A shows Rabbit anti-Human ATR.p (Threonine 1989) Recombinant Monoclonal, IgG - (BLR032P), visualized using Identifyn® SRM Alexa Fluor™ 647 Affinity Purified Donkey Anti-Rabbit, IgG (H + L), together with Rabbit anti-Human γH2Ax (Serine 139) Recombinant Monoclonal - Identifyn® SRM Alexa Fluor™ 488, IgG - (BLR014M), and DAPI nuclear counterstaining following etoposide-induced DNA damage. Relative to both conventional widefield and Apotome SIM imaging, confocal microscopy provides improved optical sectioning, enhanced axial discrimination, and reduced out-of-focus fluorescence contribution, enabling more refined visualization of ATR.p-associated DNA damage response territories throughout the nuclear volume. ATR.p demonstrated strong punctate intranuclear redistribution and damage-associated signaling structures that spatially overlapped with γH2Ax-enriched nuclear regions, consistent with coordinated replication-stress and DNA damage checkpoint activation.

Panels B and C present line-profile analysis across resolution-limited ATR.p and γH2Ax-associated foci, demonstrating strong spatial concordance and comparable fluorescence intensity distributions throughout damaged nuclei. Although confocal microscopy substantially improves volumetric and focal-plane discrimination relative to widefield and WF-SIM imaging, the observed overlap remains constrained by diffraction-limited resolution, preventing definitive nanoscale assessment of individual repair complexes or molecular organization at DNA break sites. Accordingly, the observed signal relationship should be interpreted as coordinated recruitment and overlapping damage-associated signaling territories rather than definitive molecular colocalization.

Importantly, this dataset represents the next refinement stage within the Identifyn® Stepdown Methodology™, progressively improving structural interpretation and signal discrimination prior to higher-resolution Airyscan, Lattice SIM, SIM², and STORM interrogation workflows. The transition from widefield to WF-SIM and now to confocal imaging demonstrates how incremental improvements in optical sectioning and spatial resolution progressively refine the apparent overlap between ATR.p and γH2Ax while preserving biologically coherent DNA damage response behavior across modalities.

Image Correction

For Panels B and C, which represent the line-profile analysis and the accompanying image identifying the analyzed region, the ATR.p (647) signal pair was pseudocolored white to enhance visual contrast and improve assessment of fluorescence intensity distribution, focal organization, and spatial relationships among signals across the analyzed nuclear region.

Image by J.K. Bennett
Image Analysis and Data Presentation by B.T. Bennett

© Copyright 2026 GMD12 LLC.

SOURCE PROVENANCE

Catalog	PA-RR-000013
Stage	Confocal

SOURCE PROVENANCE

Instrument	ZEISS LSM 980
Microscope configuration	Zeiss LSM980 Confocal with NIR Detection, Axio Observer.Z1/7, using a Plan-Apochromat 63x/1.40 Oil DIC M27, was used with the following paramete
Structured source metadata values	53
Metadata source	PRESERVED_SOURCE_METHOD_PDF_TEXT
Cell model	HeLa
Image SHA-256	9F030487B01B84E834E1E495FAB0FC80E2031771C05C37B7E276E77E7FE438E7
Method PDF SHA-256	0E206EF8A83B41FE69A0DD96A83FEA64FF7FC3FC820A2E42AA35A5D896E5391B

ORIGINAL IMAGE EVIDENCE / AIRYSCAN

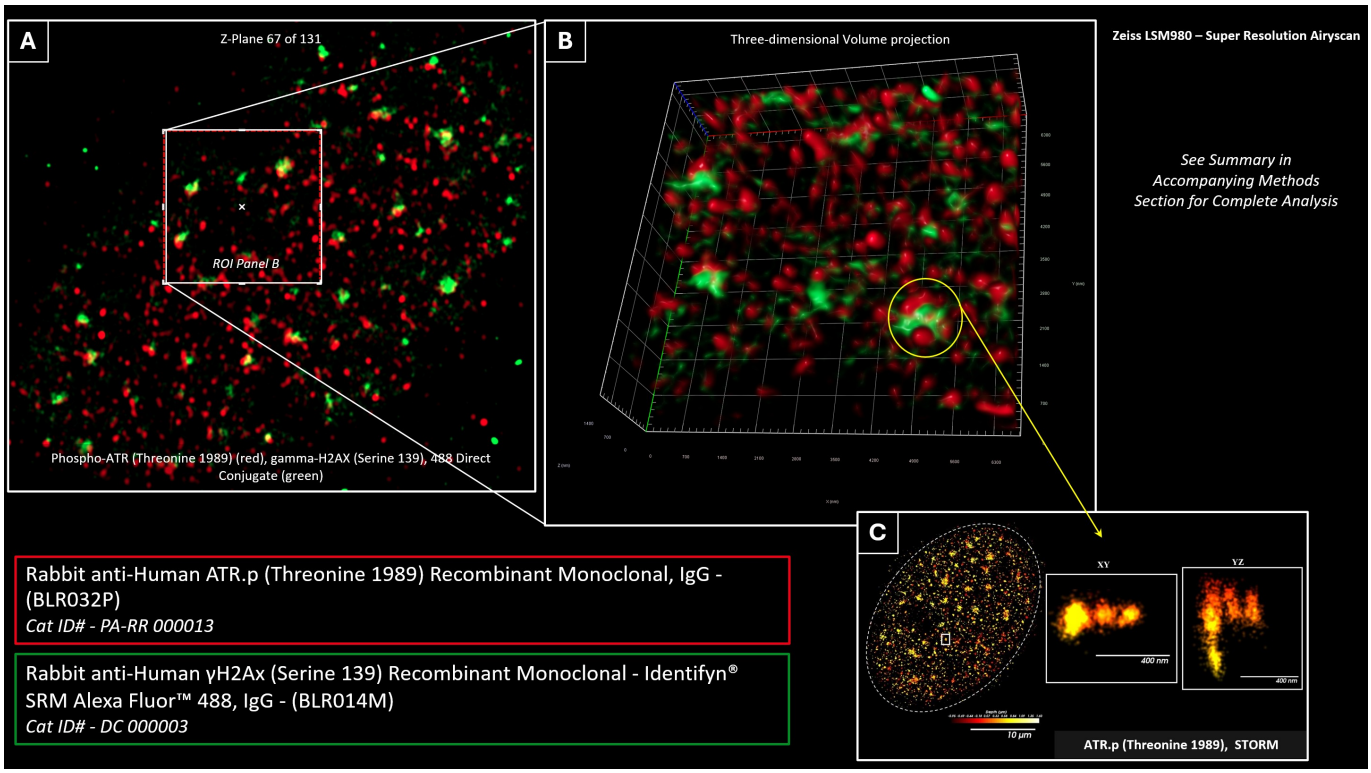

EVIDENCE TIER	Airyscan
INSTRUMENT	ZEISS LSM 980
CELL MODEL	HeLa
DETECTED DYES	405/DAPI; 488; 647; 750
METADATA VALUES	56

STRUCTURED ACQUISITION METADATA / AIRYSCAN

The values below were deterministically extracted from the preserved Identifyn method PDF text. They remain source-documented metadata, not new BENNETT measurements.

FIELD	SOURCE-DOCUMENTED VALUE
Platform / configuration	Zeiss LSM980 Confocal with NIR Detection, Axio Observer.Z1/7, using a Plan-Apochromat 63x/1.40 Oil DIC M27, was used with the following parameters for each dye:
Objective	Plan-Apochromat 63x/1.40 Oil DIC M27
Z-Stack	131 Slices (3.9 µm)
Channels	3
Scaling (Per Pixel)	0.03529 µm X 0.03530 µm X 0.03000 µm
Image Size (Pixels)	731 X 676 | 191 X 186
Image Size (Scaled)	25.80 µm X 23.86 µm | 6.74 µm X 6.56 µm
Bit Depth	16 Bit
Image Center Position	X: 95.01 mm, Y: 46.20 mm
Stage Position	X: 95.01 mm, Y: 46.20 mm
ROI Center Offset	X: 0.00 µm, Y: 0.00 µm
Reflector	None
Contrast Method	Fluorescence
Pinhole	5.00 AU / 328 µm | 5.00 AU / 250 µm | 5.00 AU / 214 µm
LMS MBS	MBS 488/639 & 405/730
LMS SBS	SBS LP 615 | SBS SP 505
Laser Wavelength	639 nm @ 2.60% | 488 nm @ 0.3% | 405 nm @ 0.3%
Laser Blanking	Enabled
Scan Mode	Frame
Scan Zoom	2.0
Rotation	0°
Sampling	2.00
Pixel Time	1.10 µs
Frame Time	18.77 s
LSM Scan Speed	6
Scan Direction	Bidirectional
Line Step	1
Averaging	4
Excitation Wavelength	653 | 493 | 353
Emission Wavelength	668 | 517 | 465
Effective NA	1.4
Detection Wavelength	643 - 735 | 499 - 548 | 422 - 477
Imaging Device	Airyscan

FIELD	SOURCE-DOCUMENTED VALUE
Detector Type	GaAsP-PMT
Detector Gain	800 V | 750 V
Detector Offset	0
Detector Digital Gain	1.0
Airyscan Mode	SuperResolution 10.0 (3D, Auto) | SuperResolution 8.5 (3D, Auto)
3D Volume Projection	Precise
Appearance	Threshold 2% all channels, Ramp 98% all channels, Maximum 100% all channels
Background	Black
Light	Brightness 100%, Azimuth 80°, Elongation -130°, Enabled Directional Lighting, Enabled Tone Mapping
Projection	View Angle 35°, Scale Z 100%, Reverse Z-Axis NOT Selected, Stereo Anaglyph NOT Selected, Camera Separation 5% (deselected), Parallax Shift 0% (deselected)

SOURCE METHOD

The text below is carried from the preserved Identifyn source record. Typography and pagination have been normalized for this preservation dossier; scientific wording has not been editorially rewritten.

Identifyn Standards for Optical Microscopy Methods™

Identifyn® Primary Antibody

Rabbit anti-Human ATR.p (Threonine 1989) Recombinant Monoclonal, IgG - (BLR032P)
Cat ID# - 000013

Rabbit anti-Human γH2Ax (Serine 139) Recombinant Monoclonal - Identifyn® SRM Alexa Fluor™ 488, IgG - (BLR014M)
Cat ID# - DC 000003

Identifyn® Secondary Antibody

Identifyn® SRM Alexa Fluor™ 647 Affinity Purified Donkey Anti-Rabbit, IgG (H + L)
Cat ID# - SA 000060

ATR (Ataxia Telangiectasia and Rad3-related) is a critical serine/threonine kinase that plays a central role in the cellular response to DNA damage, particularly in response to replication stress and single-strand breaks (SSBs). Unlike ATM (Ataxia Telangiectasia Mutated), which is primarily activated by double-strand breaks, ATR is activated by persistent single-stranded DNA (ssDNA) regions that arise during DNA replication or repair processes.
Overview of ATR Activation

ATR is activated when extensive ssDNA accumulates, often resulting from stalled replication forks or other forms of replication stress. This activation is usually mediated by RPA (Replication Protein A), which binds to ssDNA and recruits ATR and its key activator, ATRIP (ATR Interacting Protein).

Recruitment to Sites of Damage: RPA-coated ssDNA signals DNA damage or replication stress. ATR, with ATRIP, is recruited to these sites, activating ATR's kinase activity.

Interaction with the 9-1-1 Complex: ATR activation is further facilitated by the 9-1-1 complex (comprising RAD9, RAD1, and HUS1), which is loaded onto DNA by RAD17-RFC at sites of DNA damage. This complex interacts with TOPBP1 (Topoisomerase II Binding Protein 1), a key activator of ATR, thereby fully activating ATR kinase activity.

ATR's Role in Single-Strand Break Repair

ATR plays a vital role in facilitating and coordinating the repair of single-strand breaks through various mechanisms:

Checkpoint Activation: ATR is critical for activating checkpoint signaling pathways, notably by phosphorylating CHK1. This leads to cell cycle arrest or delay, allowing time for DNA repair before cell division continues. This checkpoint activation is crucial in preventing cells from progressing with unrepaired single-strand breaks.

Coordination of Repair Pathways: ATR activation helps coordinate DNA repair processes by recruiting repair proteins and integrating signals across various pathways. This coordination ensures that repair proteins involved in base excision repair (BER), homologous recombination, and other SSB-related pathways are recruited and activated as needed.

Stabilization of Replication Forks: ATR contributes to the stabilization of stalled replication forks, preventing the collapse into double-strand breaks. This is particularly important in preventing the progression of single-strand breaks into more severe DNA damage.

ATR in DNA Damage Response

Beyond its direct role in facilitating single-strand break repair, ATR has broader implications in the DNA damage response:

Genomic Stability: By ensuring proper checkpoint activation and coordinating DNA repair, ATR helps maintain genomic stability, reducing the risk of mutations and chromosomal abnormalities.

Response to Replication Stress: ATR is particularly critical in responding to replication stress, which can result in single-strand breaks due to replication fork stalling or collapse. ATR's activation in these contexts ensures that DNA repair processes are promptly initiated.

ATR is a central player in responding to single-strand breaks and replication stress, activating checkpoint pathways, coordinating DNA repair, and stabilizing replication forks. Through these functions, ATR significantly contributes to maintaining genomic stability and ensuring that cells do not progress with unrepaired DNA damage.

Method

HeLa cells were grown on acid-etched #1.5H cover glass to ~50% confluency. DNA damage was induced by treatment with 2 µM etoposide-spiked complete growth medium for 12 hours, followed by -20 °C methanol fixation and blocking with Thermo Fisher Fish Serum Blocker cat#37527X3. The primary antibody, Rabbit anti-Human ATR.p (Threonine 1989) Recombinant Monoclonal, IgG - (BLR032P), was incubated for 1 hour at room temperature at a dilution of 1:250. Cells were washed 3 times in 1X PBS. Identifyn® SRM Alexa Fluor™ 647 Affinity Purified Donkey Anti-Rabbit, IgG (H + L) was incubated at room temperature for 1 hour at a dilution of 1:1000. Cells were washed 5 times in 1X PBS.

The second primary antibody, Rabbit anti-Human γH2Ax (Serine 139) Recombinant Monoclonal - Identifyn® SRM Alexa Fluor™ 488, IgG - (BLR014M) was incubated for 1 hour at room temperature at a dilution of 1:250. Cells were washed 5 times in 1X PBS and mounted using ProLong™ Diamond Antifade Mountant with DAPI (cat# P36962).

Microscope

Zeiss LSM980 Confocal with NIR Detection, Axio Observer.Z1/7, using a Plan-Apochromat 63x/1.40 Oil DIC M27, was used with the following parameters for each dye:

Z Stack - (3D) - 2D at Z-Plane 67 of 131, Panel A

Z-Stack = 131 Slices (3.9 µm)

Channels = 3
Scaling (Per Pixel) = 0.035 nm X 0.035 nm X 0.030 nm
Image Size (Pixels) = 731 X 676
Image Size (Scaled) = 25.80 µm X 23.86 µm
Bit Depth = 16 Bit
Image Center Position = X: 95.01 mm, Y: 46.20 mm
Stage Position = X: 95.01 mm, Y: 46.20 mm
ROI Center Offset = X: 0.00 µm, Y: 0.00 µm

Z Stack - (3D) - 3D Volume Projection, Panel B

Z-Stack = 131 Slices (3.9 µm)

Channels = 3
Scaling (Per Pixel) = 0.035 nm X 0.035 nm X 0.030 nm
Image Size (Pixels) = 191 X 186
Image Size (Scaled) = 6.74 µm X 6.56 µm
Bit Depth = 16 Bit
Image Center Position = X: 95.01 mm, Y: 46.20 mm
Stage Position = X: 95.01 mm, Y: 46.20 mm
ROI Center Offset = X: 0.00 µm, Y: 0.00 µm

647 -

Reflector = None
Contrast Method = Fluorescence
Pinhole = 5.00 AU / 328 µm
LMS MBS = MBS 488/639 & 405/730
LMS SBS = SBS LP 615
Laser Wavelength = 639 nm @ 2.60%
Laser Blanking = Enabled
Scan Mode = Frame
Scan Zoom = 2.0
Rotation = 0°
Sampling = 2.00
Pixel Time = 1.10 µs
Frame Time = 18.77 s
LSM Scan Speed = 6
Scan Direction = Bidirectional
Line Step = 1
Averaging = 4
Excitation Wavelength = 653
Emission Wavelength = 668
Effective NA = 1.4
Detection Wavelength = 643 - 735
Imaging Device = Airyscan
Detector Type = GaAsP-PMT
Detector Gain = 800 V
Detector Offset = 0
Detector Digital Gain = 1.0
Airyscan Mode = SuperResolution 10.0 (3D, Auto)

488 -

Reflector = None
Contrast Method = Fluorescence
Pinhole = 5.00 AU / 250 µm
LMS MBS = MBS 488/639 & 405/730
LMS SBS = SBS SP 505
Laser Wavelength = 488 nm @ 0.3%
Laser Blanking = Enabled
Scan Mode = Frame
Scan Zoom = 2.0
Rotation = 0°
Sampling = 2.00
Pixel Time = 1.10 µs
Frame Time = 18.77 s
LSM Scan Speed = 6
Scan Direction = Bidirectional
Line Step = 1
Averaging = 4
Excitation Wavelength = 493
Emission Wavelength = 517
Effective NA = 1.4
Detection Wavelength = 499 - 548
Imaging Device = Airyscan
Detector Type = GaAsP-PMT
Detector Gain = 800 V
Detector Offset = 0
Detector Digital Gain = 1.0
Airyscan Mode = SuperResolution 10.0 (3D, Auto)

DAPI - Not Shown in Data Analysis, but Collected in Image Acquisition

Reflector = None
Contrast Method = Fluorescence
Pinhole = 5.00 AU / 214 µm
LMS MBS = MBS 488/639 & 405/730
LMS SBS = SBS SP 505
Laser Wavelength = 405 nm @ 0.3%
Laser Blanking = Enabled
Scan Mode = Frame
Scan Zoom = 2.0
Rotation = 0°
Sampling = 2.00
Pixel Time = 1.10 µs
Frame Time = 18.77 s
LSM Scan Speed = 6
Scan Direction = Bidirectional
Line Step = 1
Averaging = 4
Excitation Wavelength = 353
Emission Wavelength = 465
Effective NA = 1.4
Detection Wavelength = 422 - 477
Imaging Device = Airyscan
Detector Type = GaAsP-PMT
Detector Gain = 750 V
Detector Offset = 0
Detector Digital Gain = 1.0
Airyscan Mode = SuperResolution 8.5 (3D, Auto)

2-Dimensional View- Panel A

Shows Rabbit anti-Human ATR.p (Threonine 1989) Recombinant Monoclonal, IgG - (BLR032P), visualized using Identifyn® SRM Alexa Fluor™ 647 Affinity Purified Donkey Anti-Rabbit, IgG (H + L) secondary antibody and Rabbit anti-Human γH2Ax (Serine 139) Recombinant Monoclonal - Identifyn® SRM Alexa Fluor™ 488, IgG - (BLR014M). A Region of Interest is denoted by a white box to be further examined in the 3-Dimensional Volume Projection in Panel B.

3D Image Processing - Panel B

3D Volume Projection = Precise
Appearance = Threshold 2% all channels, Ramp 98% all channels, Maximum 100% all channels
Background = Black
Light = Brightness 100%, Azimuth 80°, Elongation -130°, Enabled Directional Lighting, Enabled Tone Mapping
Projection = View Angle 35°, Scale Z 100%, Reverse Z-Axis NOT Selected, Stereo Anaglyph NOT Selected, Camera Separation 5% (deselected), Parallax Shift 0% (deselected)

STORM - Panel C

STORM imaging from the same product dataset is shown in Panel C to demonstrate the remaining resolution limitations of Airyscan microscopy. While Airyscan provides improved sub-diffraction localization and structural discrimination relative to conventional confocal imaging, STORM imaging further resolves nanoscale organizational features and underlying damage-associated signaling architectures that are not fully distinguishable in the Airyscan dataset.

Summary

Panel A shows a single Airyscan optical section (Z-plane 67 of 131) of Rabbit anti-Human ATR.p (Threonine 1989) Recombinant Monoclonal, IgG - (BLR032P), visualized using Identifyn® SRM Alexa Fluor™ 647 Affinity Purified Donkey Anti-Rabbit, IgG (H + L), together with Rabbit anti-Human γH2Ax (Serine 139) Recombinant Monoclonal - Identifyn® SRM Alexa Fluor™ 488, IgG - (BLR014M), following etoposide-induced DNA damage. Relative to conventional widefield, WF-SIM, and confocal microscopy, Airyscan imaging provides improved sub-diffraction structural discrimination, enhanced signal localization, and increased separation of damage-associated signaling territories within the nuclear compartment. ATR.p demonstrated punctate intranuclear redistribution and spatial overlap with γH2Ax-enriched DNA damage regions, consistent with coordinated replication-stress and DNA damage checkpoint activation.

Panel B presents a three-dimensional volume reconstruction of the region of interest identified in Panel A, further illustrating the spatial organization and volumetric distribution of ATR.p and γH2Ax-associated signaling structures throughout the nuclear environment. Compared to preceding diffraction-limited modalities, Airyscan imaging reveals improved structural separation of resolution-limited aggregates and increased visualization of sub-diffraction organizational features; however, definitive nanoscale molecular architecture and precise repair-complex organization remain incompletely resolved at this imaging stage. Accordingly, the observed overlap should continue to be interpreted as coordinated recruitment and overlapping DNA damage-associated signaling territories rather than definitive molecular colocalization.

Importantly, this dataset represents the next stage of super-resolution refinement within the Identifyn® Stepdown Methodology™, demonstrating the progressive improvement in structural interpretation that accompanies increasing spatial resolution. The transition from widefield to WF-SIM, confocal, and now Airyscan imaging illustrates how incremental improvements in optical sectioning and sub-diffraction signal discrimination progressively refine ATR.p and γH2Ax-associated damage architectures prior to higher-order interrogation by Lattice SIM, SIM², and STORM imaging workflows.

Image Correction

NONE

Image by J.K. Bennett
Image Analysis and Data Presentation by B.T. Bennett

© Copyright 2026 GMD12 LLC.

SOURCE PROVENANCE

Catalog	PA-RR-000013
Stage	Airyscan

SOURCE PROVENANCE

Instrument	ZEISS LSM 980
Microscope configuration	Zeiss LSM980 Confocal with NIR Detection, Axio Observer.Z1/7, using a Plan-Apochromat 63x/1.40 Oil DIC M27, was used with the following paramete
Structured source metadata values	56
Metadata source	PRESERVED_SOURCE_METHOD_PDF_TEXT
Cell model	HeLa
Image SHA-256	1CD8A72A64D32C33B0A30697F37250878E1347009F955E43A3AE353992AD15A1
Method PDF SHA-256	83C1257F4472FE53BB208F68FE2A038BF1AA36562BF46BB165370623AC9BDC48

ORIGINAL IMAGE EVIDENCE / SIM

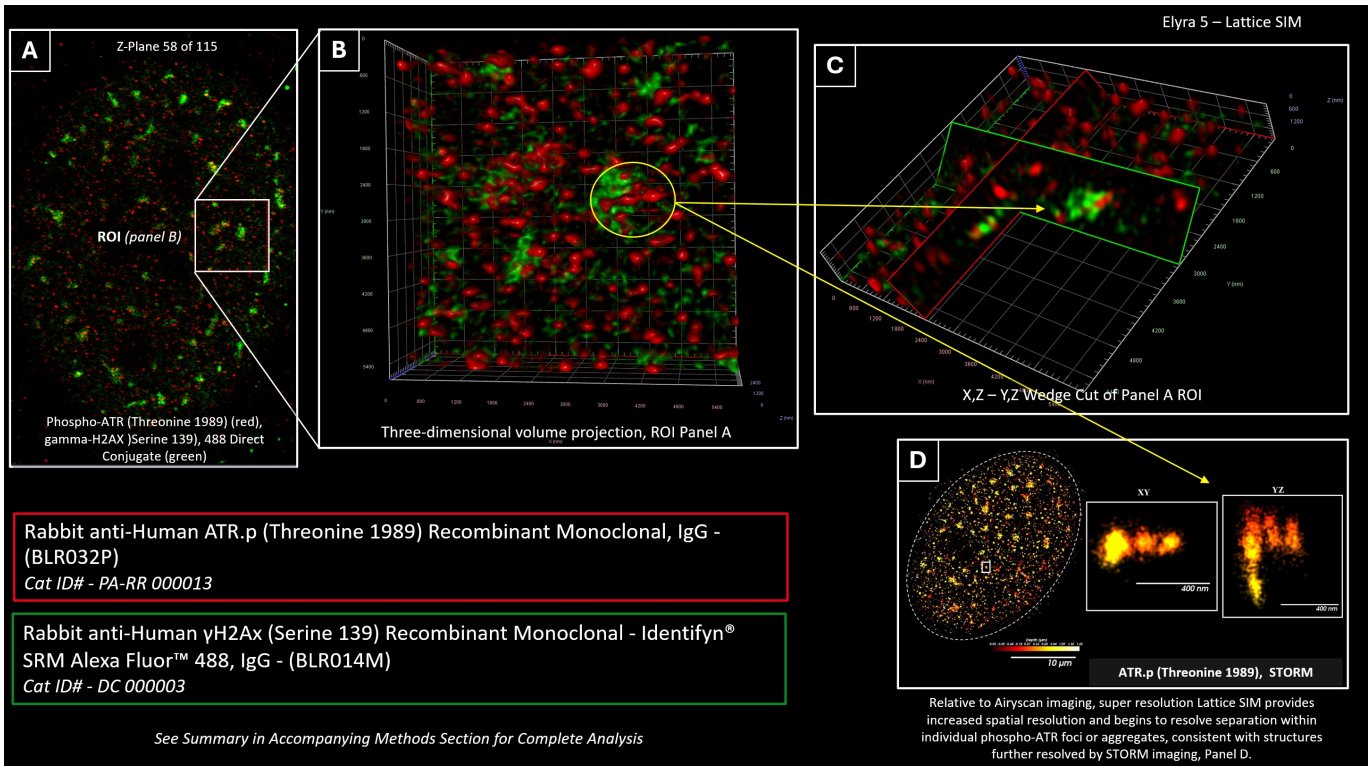

EVIDENCE TIER	SIM
INSTRUMENT	ZEISS Elyra
CELL MODEL	HeLa
DETECTED DYES	405/DAPI; 488; 647
METADATA VALUES	60

STRUCTURED ACQUISITION METADATA / SIM

The values below were deterministically extracted from the preserved Identifyn method PDF text. They remain source-documented metadata, not new BENNETT measurements.

FIELD	SOURCE-DOCUMENTED VALUE
Platform / configuration	Zeiss Elyra 5 Lattice SIM, AxioObserver.Z1/7 using Plan-Apochromat 63X/1.40 oil DIC M27, 1X Tubelens, was used with the following parameters for each dye:
Objective	Plan-Apochromat 63X/1.40 oil DIC M27
Z-Stack	115 Slices (3.42 µm)
Channels	3 | 2
Scaling (Per Pixel)	0.02111 µm X 0.02111 µm X 0.02974 µm
Image Size (Pixels)	1145 X 1654 | 275 X 268
Image Size (Scaled)	24.17 µm X 34.92 µm | 5.81 µm X 5.66 µm
Bit Depth	16 Bit
Image Center Position	X: 69.03 mm, Y: 39.62 mm
Stage Position	X: 69.03 mm, Y: 39.62 mm
ROI Center Offset	X: 0.00 µm, Y: 0.00 µm
Reflectors	SR HE LBF 405/488/561/642
Beam Splitter	405, 488, 561, 642
Filter Excitation Wavelength	200 - 405, 200 - 488, 200 - 561, 200 - 642
Filter Emission Wavelength	419 - 470, 503 - 546, 576 - 617, 657 - 800
Contrast Method	Fluorescence
Illumination Wavelength	640 | 488
Channel Name	T1-Axiocam 820 -SR | T2-Axiocam 820-SR
Excitation Wavelength	640 | 488
Emission Wavelength	729 | 525
Effective NA	1.4
Detection Wavelength	419 - 470, 503 - 546, 576 - 617, 657 - 800
Imaging Device	Axiocam 820
Camera Adapter	1X
Exposure Time	120 ms
Depth of Focus	1.13 µm | 0.81 µm
Binning Mode	2,2
Laser Wavelength	640 nm @ 3.5% | 488 nm @ 0.50%
Frame Time	1.59 s
Scan Direction	Unidirectional
Grating	36.5 µm grating | 27.5 µm grating
Processing Dimension	3D
Result Sampling	4

FIELD	SOURCE-DOCUMENTED VALUE
Process Sampling	N/A
Algorithm	SIM
SIM Settings	Standard
Auto Sharpness	On
Sharpness	11.3281 (647), 11.2313 (488)
Fitting	Fast Fit
Normalization	Auto
3D Volume Projection	Precise
Appearance	Threshold 2% all channels, Ramp 98% all channels, Maximum 100% all channels
Background	Black
Light	Brightness 100%, Azimuth 80°, Elongation -130°, Enabled Directional Lighting, Enabled Tone Mapping
Projection	View Angle 35°, Scale Z 75%, Reverse Z-Axis NOT Selected, Stereo Anaglyph NOT Selected, Camera Separation 5% (deselected), Parallax Shift 0% (deselected)
X-Z	Activate was selected, textured opaque was chosen, and a green outline of the clipped perimeter was shown; Clip Back was selected, and Clip Front was NOT selected.
Position of Clip	-8% | -27%
Clip Y	-30° | 15°
Clip Z	0°
Y-Z	Activate was selected, textured opaque was chosen, and a red outline of the clipped perimeter was shown; Clip Back was selected, and Clip Front was NOT selected.

SOURCE METHOD

The text below is carried from the preserved Identifyn source record. Typography and pagination have been normalized for this preservation dossier; scientific wording has not been editorially rewritten.

Identifyn Standards for Optical Microscopy Methods™

Identifyn® Primary Antibody

Rabbit anti-Human ATR.p (Threonine 1989) Recombinant Monoclonal, IgG - (BLR032P)
Cat ID# - 000013

Rabbit anti-Human γH2Ax (Serine 139) Recombinant Monoclonal - Identifyn® SRM Alexa Fluor™ 488, IgG - (BLR014M)
Cat ID# - DC 000003

Identifyn® Secondary Antibody

Identifyn® SRM Alexa Fluor™ 647 Affinity Purified Donkey Anti-Rabbit, IgG (H + L)
Cat ID# - SA 000060

ATR (Ataxia Telangiectasia and Rad3-related) is a critical serine/threonine kinase that plays a central role in the cellular response to DNA damage, particularly in response to replication stress and single-strand breaks (SSBs). Unlike ATM (Ataxia Telangiectasia Mutated), which is primarily activated by double-strand breaks, ATR is activated by persistent single-stranded DNA (ssDNA) regions that arise during DNA replication or repair processes.
Overview of ATR Activation

ATR is activated when extensive ssDNA accumulates, often resulting from stalled replication forks or other forms of replication stress. This activation is usually mediated by RPA (Replication Protein A), which binds to ssDNA and recruits ATR and its key activator, ATRIP (ATR Interacting Protein).

Recruitment to Sites of Damage: RPA-coated ssDNA signals DNA damage or replication stress. ATR, with ATRIP, is recruited to these sites, activating ATR's kinase activity.

Interaction with the 9-1-1 Complex: ATR activation is further facilitated by the 9-1-1 complex (comprising RAD9, RAD1, and HUS1), which is loaded onto DNA by RAD17-RFC at sites of DNA damage. This complex interacts with TOPBP1 (Topoisomerase II Binding Protein 1), a key activator of ATR, thereby fully activating ATR kinase activity.

ATR's Role in Single-Strand Break Repair

ATR plays a vital role in facilitating and coordinating the repair of single-strand breaks through various mechanisms:

Checkpoint Activation: ATR is critical for activating checkpoint signaling pathways, notably by phosphorylating CHK1. This leads to cell cycle arrest or delay, allowing time for DNA repair before cell division continues. This checkpoint activation is crucial in preventing cells from progressing with unrepaired single-strand breaks.

Coordination of Repair Pathways: ATR activation helps coordinate DNA repair processes by recruiting repair proteins and integrating signals across various pathways. This coordination ensures that repair proteins involved in base excision repair (BER), homologous recombination, and other SSB-related pathways are recruited and activated as needed.

Stabilization of Replication Forks: ATR contributes to the stabilization of stalled replication forks, preventing the collapse into double-strand breaks. This is particularly important in preventing the progression of single-strand breaks into more severe DNA damage.

ATR in DNA Damage Response

Beyond its direct role in facilitating single-strand break repair, ATR has broader implications in the DNA damage response:

Genomic Stability: By ensuring proper checkpoint activation and coordinating DNA repair, ATR helps maintain genomic stability, reducing the risk of mutations and chromosomal abnormalities.

Response to Replication Stress: ATR is particularly critical in responding to replication stress, which can result in single-strand breaks due to replication fork stalling or collapse. ATR's activation in these contexts ensures that DNA repair processes are promptly initiated.

ATR is a central player in responding to single-strand breaks and replication stress, activating checkpoint pathways, coordinating DNA repair, and stabilizing replication forks. Through these functions, ATR significantly contributes to maintaining genomic stability and ensuring that cells do not progress with unrepaired DNA damage.

Method

HeLa cells were grown on acid-etched #1.5H cover glass to ~50% confluency. DNA damage was induced by treatment with 2 µM etoposide-spiked complete growth medium for 12 hours, followed by -20 °C methanol fixation and blocking with Thermo Fisher Fish Serum Blocker cat#37527X3. The primary antibody, Rabbit anti-Human ATR.p (Threonine 1989) Recombinant Monoclonal, IgG - (BLR032P), was incubated for 1 hour at room temperature at a dilution of 1:250. Cells were washed 3 times in 1X PBS. Identifyn® SRM Alexa Fluor™ 647 Affinity Purified Donkey Anti-Rabbit, IgG (H + L) was incubated at room temperature for 1 hour at a dilution of 1:1000. Cells were washed 5 times in 1X PBS.

The second primary antibody, Rabbit anti-Human γH2Ax (Serine 139) Recombinant Monoclonal - Identifyn® SRM Alexa Fluor™ 488, IgG - (BLR014M) was incubated for 1 hour at room temperature at a dilution of 1:250. Cells were washed 5 times in 1X PBS and mounted using ProLong™ Diamond Antifade Mountant with DAPI (cat# P36962).

Microscope

Zeiss Elyra 5 Lattice SIM, AxioObserver.Z1/7 using Plan-Apochromat 63X/1.40 oil DIC M27, 1X Tubelens, was used with the following parameters for each dye:

Z Stack - (3D) - 2D at Z-Plane 58 of 115, Panel A

Z-Stack = 115 Slices (3.42 µm)

Channels = 3
Scaling (Per Pixel) = 0.021 nm X 0.021 nm X 0.030 nm
Image Size (Pixels) = 1145 X 1654
Image Size (Scaled) = 24.17 µm X 34.92 µm
Bit Depth = 16 Bit
Image Center Position = X: 69.03 mm, Y: 39.62 mm
Stage Position = X: 69.03 mm, Y: 39.62 mm
ROI Center Offset = X: 0.00 µm, Y: 0.00 µm

Z Stack - (3D) - 3D Volume Projection, Panels B and C

Z-Stack = 115 Slices (3.42 µm)

Channels = 3
Scaling (Per Pixel) = 0.021 nm X 0.021 nm X 0.030 nm
Image Size (Pixels) = 275 X 268
Image Size (Scaled) = 5.81 µm X 5.66 µm
Bit Depth = 16 Bit
Image Center Position = X: 69.03 mm, Y: 39.62 mm
Stage Position = X: 69.03 mm, Y: 39.62 mm
ROI Center Offset = X: 0.00 µm, Y: 0.00 µm

647 -

Reflectors = SR HE LBF 405/488/561/642
Beam Splitter = 405, 488, 561, 642
Filter Excitation Wavelength = 200 - 405, 200 - 488, 200 - 561, 200 - 642
Filter Emission Wavelength = 419 - 470, 503 - 546, 576 - 617, 657 - 800
Contrast Method = Fluorescence
Illumination Wavelength = 640
Channel Name = T1-Axiocam 820 -SR
Excitation Wavelength = 640
Emission Wavelength = 729
Effective NA = 1.4
Detection Wavelength = 419 - 470, 503 - 546, 576 - 617, 657 - 800
Imaging Device = Axiocam 820
Camera Adapter = 1X
Exposure Time = 120 ms
Depth of Focus = 1.13 µm
Binning Mode = 2,2
Laser Wavelength = 640 nm @ 3.5%
Frame Time = 1.59 s
Scan Direction = Unidirectional
Grating = 36.5 µm grating

488 -

Reflectors = SR HE LBF 405/488/561/642
Beam Splitter = 405, 488, 561, 642
Filter Excitation Wavelength = 200 - 405, 200 - 488, 200 - 561, 200 - 642
Filter Emission Wavelength = 419 - 470, 503 - 546, 576 - 617, 657 - 800
Contrast Method = Fluorescence
Illumination Wavelength = 488
Channel Name = T2-Axiocam 820-SR
Excitation Wavelength = 488
Emission Wavelength = 525
Effective NA = 1.4
Detection Wavelength = 419 - 470, 503 - 546, 576 - 617, 657 - 800
Imaging Device = Axiocam 820
Camera Adapter = 1X
Exposure Time = 120 ms
Depth of Focus = 0.81 µm
Binning Mode = 2,2
Laser Wavelength = 488 nm @ 0.50%
Frame Time = 1.59 s
Scan Direction = Unidirectional
Grating = 27.5 µm grating

Post Processing - SIM Processing

Processing Dimension = 3D
Result Sampling = 4
Process Sampling = N/A
Channels = 2
Algorithm = SIM
SIM Settings = Standard
Auto Sharpness = On
Sharpness = 11.3281 (647), 11.2313 (488)
Fitting = Fast Fit
Normalization = Auto

2-Dimensional View- Panel A

Shows Rabbit anti-Human ATR.p (Threonine 1989) Recombinant Monoclonal, IgG - (BLR032P), visualized using Identifyn® SRM Alexa Fluor™ 647 Affinity Purified Donkey Anti-Rabbit, IgG (H + L) secondary antibody and Rabbit anti-Human γH2Ax (Serine 139) Recombinant Monoclonal - Identifyn® SRM Alexa Fluor™ 488, IgG - (BLR014M). A Region of Interest is denoted by a white box to be further examined in the 3-Dimensional Volume Projection in Panel B and C.

3D Image Processing - Panel B

3D Volume Projection = Precise
Appearance = Threshold 2% all channels, Ramp 98% all channels, Maximum 100% all channels
Background = Black
Light = Brightness 100%, Azimuth 80°, Elongation -130°, Enabled Directional Lighting, Enabled Tone Mapping
Projection = View Angle 35°, Scale Z 75%, Reverse Z-Axis NOT Selected, Stereo Anaglyph NOT Selected, Camera Separation 5% (deselected), Parallax Shift 0% (deselected)

Clipping Image Process - Panel B

Clipping planes are introduced in Panel C to highlight the Rabbit anti-Human Phospho-ATR (Threonine 19189) Recombinant Monoclonal and gamma-H2AX (Serine 139)488 Direct Conjugate within the nuclear compartment by adjusting or cutting away portions of the image using a triple-wedge cut, removing parts of the image in the X-Z and Y-Z planes.

X-Z = Activate was selected, textured opaque was chosen, and a green outline of the clipped perimeter was shown; Clip Back was selected, and Clip Front was NOT selected.

Position of Clip = -8%
Clip Y = -30°
Clip Z = 0°

Y-Z = Activate was selected, textured opaque was chosen, and a red outline of the clipped perimeter was shown; Clip Back was selected, and Clip Front was NOT selected.

Position of Clip = -27%
Clip Y = 15°
Clip Z = 0°

Panel C shows a wedge-cut view displayed from the top with a slight backward rotation, highlighting the region of wedge removal and revealing the full depth of signal distribution across the z-stack. This orientation provides an alternative view of wedge geometry. It supports intranuclear overlap, coordinated recruitment, and improved sub-diffraction structural discrimination of ATR.p and γH2Ax-associated DNA damage signaling territories relative to preceding imaging modalities.

Storm - Panel C

Imaging from the same product dataset is shown in Panel C to demonstrate the remaining resolution limitations of Lattice SIM microscopy. While Lattice SIM provides improved sub-diffraction localization and structural discrimination relative to Airyscan imaging, STORM further resolves nanoscale organizational features and the underlying DNA damage-associated signaling architectures that are not fully distinguishable in the Lattice SIM dataset. Importantly, the observed signal distribution and structural organization remain highly consistent with the preceding Airyscan data while beginning to approximate the single-molecule localization patterns visualized by STORM imaging more closely.

Summary

Panel A shows a single Lattice SIM optical section (Z-plane 58 of 115) of Rabbit anti-Human ATR.p (Threonine 1989) Recombinant Monoclonal, IgG - (BLR032P), visualized using Identifyn® SRM Alexa Fluor™ 647 Affinity Purified Donkey Anti-Rabbit, IgG (H + L), together with Rabbit anti-Human γH2Ax (Serine 139) Recombinant Monoclonal - Identifyn® SRM Alexa Fluor™ 488, IgG - (BLR014M), following etoposide-induced DNA damage. Relative to conventional widefield, WF-SIM, confocal, and Airyscan imaging, Lattice SIM provides substantially improved sub-diffraction structural discrimination and enhanced visualization of punctate DNA damage-associated signaling architectures within the nuclear compartment. ATR.p demonstrated highly organized intranuclear redistribution patterns and spatial overlap with γH2Ax-enriched damage territories, consistent with coordinated replication-stress signaling and DNA damage checkpoint activation.

Panels B and C present three-dimensional volume reconstruction and wedge-cut clipping-plane analysis of the region of interest identified in Panel A, allowing improved interrogation of signal organization throughout the z-stack. Compared with preceding modalities, Lattice SIM imaging reveals increased structural separation of resolution-limited signaling aggregates and improved visualization of sub-diffractional organizational features associated with ATR.p and γH2Ax recruitment. Although the observed overlap and structural refinement strongly support coordinated recruitment

within shared DNA damage-associated nuclear territories, definitive nanoscale molecular architecture and precise repair-complex organization remain incompletely resolved at this imaging stage. Accordingly, the observed signal relationship should continue to be interpreted as coordinated recruitment and overlapping damage-associated signaling territories rather than definitive molecular colocalization.

Importantly, this dataset represents a major super-resolution refinement stage within the Identifyn® Stepdown Methodology™, demonstrating progressively improved structural interpretation as spatial resolution increases across modalities. The transition from widefield to WF-SIM, confocal, Airyscan, and now Lattice SIM imaging illustrates the progressive emergence of increasingly discrete ATR.p and γH2Ax-associated signaling architectures prior to final nanoscale interrogation using SIM² and single-molecule STORM imaging workflows.

Image Correction

NONE

Image by J. H. Cheong
Image Analysis and Data Presentation by B.T. Bennett

© Copyright 2026 GMD12 LLC.

SOURCE PROVENANCE

Catalog	PA-RR-000013
Stage	SIM
Instrument	ZEISS Elyra
Microscope configuration	Zeiss Elyra 5 Lattice SIM, AxioObserver.Z1/7 using Plan-Apochromat 63X/1.40 oil DIC M27, 1X Tubelens, was used with the following parameters for e
Structured source metadata values	60
Metadata source	PRESERVED_SOURCE_METHOD_PDF_TEXT
Cell model	HeLa
Image SHA-256	0ED8C6C1586157BD475FD984C6DD000E1E3BC9246C948DF9498E3B2E1CF20CCD
Method PDF SHA-256	CAF15A0ADAC8E68F3BA2EC8F67C31E6A86EDFC6EE8A03E9533214EF192EAE89F

ORIGINAL IMAGE EVIDENCE / SIM²

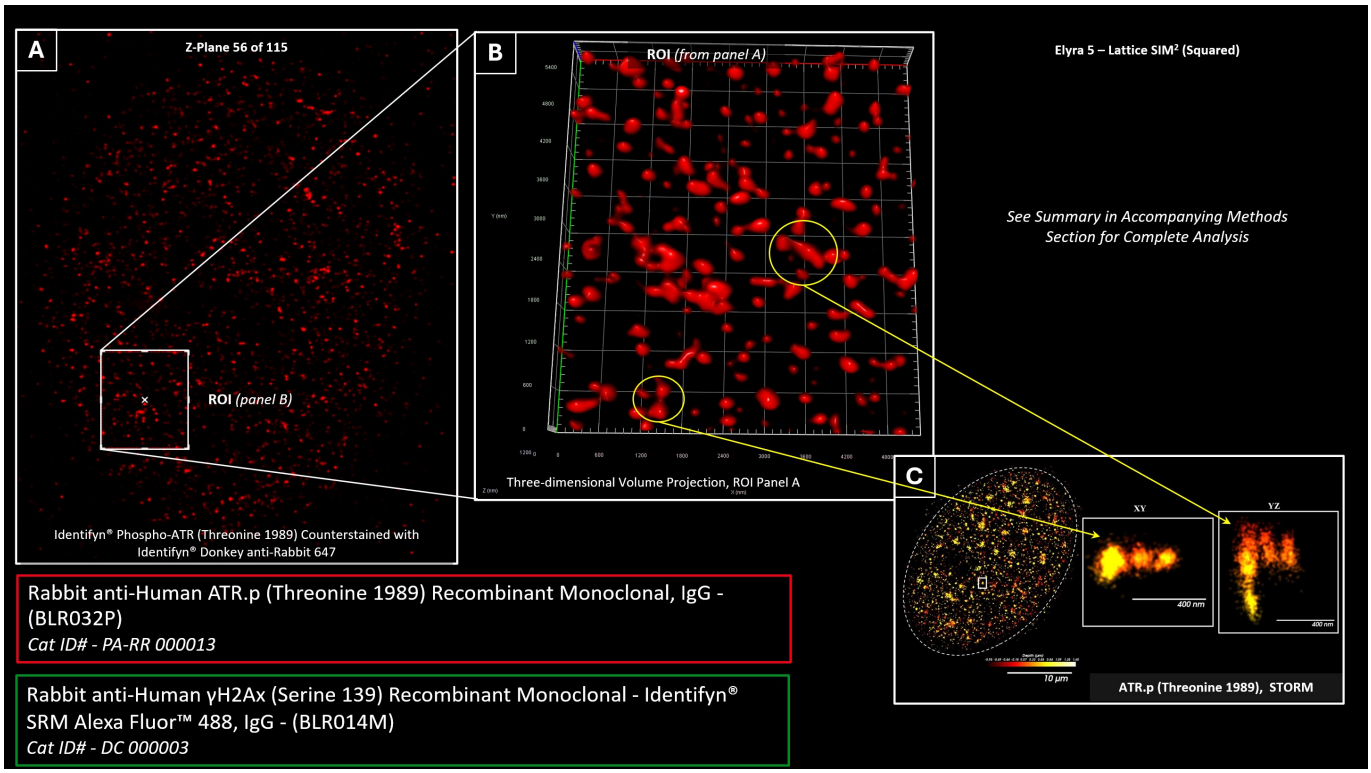

EVIDENCE TIER	SIM²
INSTRUMENT	ZEISS Elyra
CELL MODEL	HeLa
DETECTED DYES	405/DAPI; 488; 647
METADATA VALUES	53

STRUCTURED ACQUISITION METADATA / SIM²

The values below were deterministically extracted from the preserved Identifyn method PDF text. They remain source-documented metadata, not new BENNETT measurements.

FIELD	SOURCE-DOCUMENTED VALUE
Platform / configuration	Zeiss Elyra 5 Lattice SIM, AxioObserver.Z1/7 using Plan-Apochromat 63X/1.40 oil DIC M27, 1X Tubelens, was used with the following parameters for each dye:
Objective	Plan-Apochromat 63X/1.40 oil DIC M27
Z-Stack	115 Slices (3.42 µm)
Channels	3 | 2
Scaling (Per Pixel)	0.02112 µm X 0.02111 µm X 0.02974 µm
Image Size (Pixels)	1374 X 194 | 250 X 280
Image Size (Scaled)	29.01 µm X 35.76 µm | 5.28 µm X 5.91 µm
Bit Depth	16 Bit
Image Center Position	X: 69.03 mm, Y: 39.62 mm
Stage Position	X: 69.03 mm, Y: 39.62 mm
ROI Center Offset	X: 0.00 µm, Y: 0.00 µm
Reflectors	SR HE LBF 405/488/561/642
Beam Splitter	405, 488, 561, 642
Filter Excitation Wavelength	200 - 405, 200 - 488, 200 - 561, 200 - 642
Filter Emission Wavelength	419 - 470, 503 - 546, 576 - 617, 657 - 800
Contrast Method	Fluorescence
Illumination Wavelength	640 | 488
Channel Name	T1-Axiocam 820 -SR | T2-Axiocam 820-SR
Excitation Wavelength	640 | 488
Emission Wavelength	729 | 525
Effective NA	1.4
Detection Wavelength	419 - 470, 503 - 546, 576 - 617, 657 - 800
Imaging Device	Axiocam 820
Camera Adapter	1X
Exposure Time	120 ms
Depth of Focus	1.13 µm | 0.81 µm
Binning Mode	2,2
Laser Wavelength	640 nm @ 3.5% | 488 nm @ 0.50%
Frame Time	1.59 s
Scan Direction	Unidirectional
Grating	36.5 µm grating | 27.5 µm grating
Result Sampling	4
Process Sampling	4

FIELD	SOURCE-DOCUMENTED VALUE
Algorithm	SIM2
Input SNR	Low
Regularization Weight	0.0000
Iterations	3
Filter	No Filter
Fitting	Fast Fit
Normalization	Auto
3D Volume Projection	Precise
Appearance	Threshold 2% all channels, Ramp 98% all channels, Maximum 100% all channels
Background	Black
Light	Brightness 100%, Azimuth 80°, Elongation -130°, Enabled Directional Lighting, Enabled Tone Mapping
Projection	View Angle 35°, Scale Z 10%, Reverse Z-Axis NOT Selected, Stereo Anaglyph NOT Selected, Camera Separation 5% (deselected), Parallax Shift 0% (deselected)

SOURCE METHOD

The text below is carried from the preserved Identifyn source record. Typography and pagination have been normalized for this preservation dossier; scientific wording has not been editorially rewritten.

Identifyn Standards for Optical Microscopy Methods™

Identifyn® Primary Antibody

Rabbit anti-Human ATR.p (Threonine 1989) Recombinant Monoclonal, IgG - (BLR032P)
Cat ID# - 000013

Rabbit anti-Human γH2Ax (Serine 139) Recombinant Monoclonal - Identifyn® SRM Alexa Fluor™ 488, IgG - (BLR014M)
Cat ID# - DC 000003

Identifyn® Secondary Antibody

Identifyn® SRM Alexa Fluor™ 647 Affinity Purified Donkey Anti-Rabbit, IgG (H + L)
Cat ID# - SA 000060

ATR (Ataxia Telangiectasia and Rad3-related) is a critical serine/threonine kinase that plays a central role in the cellular response to DNA damage, particularly in response to replication stress and single-strand breaks (SSBs). Unlike ATM (Ataxia Telangiectasia Mutated), which is primarily activated by double-strand breaks, ATR is activated by persistent single-stranded DNA (ssDNA) regions that arise during DNA replication or repair processes.
Overview of ATR Activation

ATR is activated when extensive ssDNA accumulates, often resulting from stalled replication forks or other forms of replication stress. This activation is usually mediated by RPA (Replication Protein A), which binds to ssDNA and recruits ATR and its key activator, ATRIP (ATR Interacting Protein).

Recruitment to Sites of Damage: RPA-coated ssDNA signals DNA damage or replication stress. ATR, with ATRIP, is recruited to these sites, activating ATR's kinase activity.

Interaction with the 9-1-1 Complex: ATR activation is further facilitated by the 9-1-1 complex (comprising RAD9, RAD1, and HUS1), which is loaded onto DNA by RAD17-RFC at sites of DNA damage. This complex interacts with TOPBP1 (Topoisomerase II Binding Protein 1), a key activator of ATR, thereby fully activating ATR kinase activity.

ATR's Role in Single-Strand Break Repair

ATR plays a vital role in facilitating and coordinating the repair of single-strand breaks through various mechanisms:

Checkpoint Activation: ATR is critical for activating checkpoint signaling pathways, notably by phosphorylating CHK1. This leads to cell cycle arrest or delay, allowing time for DNA repair before cell division continues. This checkpoint activation is crucial in preventing cells from progressing with unrepaired single-strand breaks.

Coordination of Repair Pathways: ATR activation helps coordinate DNA repair processes by recruiting repair proteins and integrating signals across various pathways. This coordination ensures that repair proteins involved in base excision repair (BER), homologous recombination, and other SSB-related pathways are recruited and activated as needed.

Stabilization of Replication Forks: ATR contributes to the stabilization of stalled replication forks, preventing the collapse into double-strand breaks. This is particularly important in preventing the progression of single-strand breaks into more severe DNA damage.

ATR in DNA Damage Response

Beyond its direct role in facilitating single-strand break repair, ATR has broader implications in the DNA damage response:

Genomic Stability: By ensuring proper checkpoint activation and coordinating DNA repair, ATR helps maintain genomic stability, reducing the risk of mutations and chromosomal abnormalities.

Response to Replication Stress: ATR is particularly critical in responding to replication stress, which can result in single-strand breaks due to replication fork stalling or collapse. ATR's activation in these contexts ensures that DNA repair processes are promptly initiated.

ATR is a central player in responding to single-strand breaks and replication stress, activating checkpoint pathways, coordinating DNA repair, and stabilizing replication forks. Through these functions, ATR significantly contributes to maintaining genomic stability and ensuring that cells do not progress with unrepaired DNA damage.

Method

HeLa cells were grown on acid-etched #1.5H cover glass to ~50% confluency. DNA damage was induced by treatment with 2 μM etoposide-spiked complete growth medium for 12 hours, followed by -20 °C methanol fixation and blocking with Thermo Fisher Fish Serum Blocker cat#37527X3. The primary antibody, Rabbit anti-Human ATR.p (Threonine 1989) Recombinant Monoclonal, IgG - (BLR032P), was incubated for 1 hour at room temperature at a dilution of 1:250. Cells were washed 3 times in 1X PBS. Identifyn® SRM Alexa Fluor™ 647 Affinity Purified Donkey Anti-Rabbit, IgG (H + L) was incubated at room temperature for 1 hour at a dilution of 1:1000. Cells were washed 5 times in 1X PBS.

The second primary antibody, Rabbit anti-Human γH2Ax (Serine 139) Recombinant Monoclonal - Identifyn® SRM Alexa Fluor™ 488, IgG - (BLR014M) was incubated for 1 hour at room temperature at a dilution of 1:250. Cells were washed 5 times in 1X PBS and mounted using ProLong™ Diamond Antifade Mountant with DAPI (cat# P36962).

Microscope

Zeiss Elyra 5 Lattice SIM, AxioObserver.Z1/7 using Plan-Apochromat 63X/1.40 oil DIC M27, 1X Tubelens, was used with the following parameters for each dye:

Z Stack - (3D) - 2D at Z-Plane 56 of 115, Panel A

Z-Stack = 115 Slices (3.42 μm)

Channels = 3
Scaling (Per Pixel) = 0.021 nm X 0.021 nm X 0.030 nm
Image Size (Pixels) = 1374 X 194
Image Size (Scaled) = 29.01 μm X 35.76 μm
Bit Depth = 16 Bit
Image Center Position = X: 69.03 mm, Y: 39.62 mm
Stage Position = X: 69.03 mm, Y: 39.62 mm
ROI Center Offset = X: 0.00 μm, Y: 0.00 μm

Z Stack - (3D) - 3D Volume Projection, Panel B

Z-Stack = 115 Slices (3.42 µm)

Channels = 3
Scaling (Per Pixel) = 0.021 nm X 0.021 nm X 0.030 nm
Image Size (Pixels) = 250 X 280
Image Size (Scaled) = 5.28 µm X 5.91 µm
Bit Depth = 16 Bit
Image Center Position = X: 69.03 mm, Y: 39.62 mm
Stage Position = X: 69.03 mm, Y: 39.62 mm
ROI Center Offset = X: 0.00 µm, Y: 0.00 µm

647 -

Reflectors = SR HE LBF 405/488/561/642
Beam Splitter = 405, 488, 561, 642
Filter Excitation Wavelength = 200 - 405, 200 - 488, 200 - 561, 200 - 642
Filter Emission Wavelength = 419 - 470, 503 - 546, 576 - 617, 657 - 800
Contrast Method = Fluorescence
Illumination Wavelength = 640
Channel Name = T1-Axiocam 820 -SR
Excitation Wavelength = 640
Emission Wavelength = 729
Effective NA = 1.4
Detection Wavelength = 419 - 470, 503 - 546, 576 - 617, 657 - 800
Imaging Device = Axiocam 820
Camera Adapter = 1X
Exposure Time = 120 ms
Depth of Focus = 1.13 µm
Binning Mode = 2,2
Laser Wavelength = 640 nm @ 3.5%
Frame Time = 1.59 s
Scan Direction = Unidirectional
Grating = 36.5 µm grating

488 - Collected in Image Acquisition but not Shown in this Analysis

Reflectors = SR HE LBF 405/488/561/642
Beam Splitter = 405, 488, 561, 642
Filter Excitation Wavelength = 200 - 405, 200 - 488, 200 - 561, 200 - 642
Filter Emission Wavelength = 419 - 470, 503 - 546, 576 - 617, 657 - 800
Contrast Method = Fluorescence
Illumination Wavelength = 488
Channel Name = T2-Axiocam 820-SR
Excitation Wavelength = 488
Emission Wavelength = 525
Effective NA = 1.4
Detection Wavelength = 419 - 470, 503 - 546, 576 - 617, 657 - 800
Imaging Device = Axiocam 820
Camera Adapter = 1X
Exposure Time = 120 ms
Depth of Focus = 0.81 µm
Binning Mode = 2,2
Laser Wavelength = 488 nm @ 0.50%
Frame Time = 1.59 s
Scan Direction = Unidirectional
Grating = 27.5 µm grating

Post Processing - SIM2 Processing

Processing Dimension - 3D
Result Sampling = 4
Process Sampling = 4
Channels = 2
Algorithm = SIM2
Input SNR = Low
Regularization Weight = 0.0000
Iterations = 3
Filter = No Filter
Fitting = Fast Fit
Normalization = Auto

2-Dimensional View- Panel A

Shows Rabbit anti-Human ATR.p (Threonine 1989) Recombinant Monoclonal, IgG - (BLR032P), visualized using Identifyn® SRM Alexa Fluor™ 647 Affinity Purified Donkey Anti-Rabbit, IgG (H + L) secondary antibody. A Region of Interest is denoted by a white box to be further examined in the 3-Dimensional Volume Projection in Panel B.

3D Image Processing - Panel B

3D Volume Projection = Precise
Appearance = Threshold 2% all channels, Ramp 98% all channels, Maximum 100% all channels
Background = Black
Light = Brightness 100%, Azimuth 80°, Elongation -130°, Enabled Directional Lighting, Enabled Tone Mapping
Projection = View Angle 35°, Scale Z 10%, Reverse Z-Axis NOT Selected, Stereo Anaglyph NOT Selected, Camera Separation 5% (deselected), Parallax Shift 0% (deselected)

STORM - Panel C

STORM imaging from the same product dataset is shown in Panel C to demonstrate the remaining resolution limitations of Lattice SIM² microscopy. Using SIM² super-resolution imaging, structures that appear as single foci under confocal and Airyscan conditions become increasingly resolved into spatially distinct signaling architectures, with Lattice SIM² providing additional refinement of sub-diffraction-resolution structural organization compared with conventional Lattice SIM imaging. However, only modest additional structural discrimination is achieved when progressing from SIM to SIM², highlighting the diminishing structural gains prior to the transition to single-molecule localization microscopy.

In contrast, STORM imaging provides substantially enhanced nanoscale structural resolution, revealing fine ATR.p-associated signaling architectures and sub-diffraction organizational features not fully distinguishable within the SIM² dataset. Importantly, although structural patterns observed in SIM² show reproducible similarities to those visualized by STORM, any apparent correspondence between modalities is inferential, and caution is warranted when extrapolating structural equivalence across imaging scales. Moreover, while STORM substantially improves nanoscale visualization, additional unresolved substructure likely remains below the modality's effective resolution limits.

Summary

Panel A shows a single SIM² optical section (Z-plane 56 of 115) of Rabbit anti-Human ATR.p (Threonine 1989) Recombinant Monoclonal, IgG - (BLR032P), visualized using Identifyn® SRM Alexa Fluor™ 647 Affinity Purified Donkey Anti-Rabbit, IgG (H + L), following etoposide-induced DNA damage. Relative to conventional widefield, WF-SIM, confocal, Airyscan, and Lattice SIM imaging, SIM² provides further refinement of sub-diffraction structural discrimination and improved visualization of punctate ATR.p-associated signaling architectures within the nuclear compartment. Distinct intranuclear signaling structures become increasingly separable from broader resolution-limited aggregates observed in preceding modalities, supporting progressively refined interpretation of ATR.p-associated DNA damage response organization.

Panel B presents a three-dimensional volume reconstruction of the region of interest identified in Panel A, further illustrating the volumetric distribution and structural organization of ATR.p-associated signaling territories throughout the z-stack. Relative to preceding modalities, SIM² imaging demonstrates improved separation and refinement of sub-diffraction signaling structures while simultaneously emphasizing the remaining limitations of diffraction-based super-resolution imaging approaches. Although reproducible similarities emerge between SIM² and STORM-associated structural patterns, the definitive molecular architecture and precise nanoscale organization of repair complexes remain incompletely resolved at this imaging stage. Accordingly, the observed signal organization should continue to be interpreted as progressively refined structural discrimination of ATR.p-associated damage territories rather than definitive molecular equivalence to single-molecule localization datasets.

Importantly, this dataset represents one of the final super-resolution refinement stages within the Identifyn® Stepdown Methodology™, demonstrating the progressive emergence of increasingly discrete ATR.p-associated signaling architectures as imaging resolution advances across modalities. The transition from widefield to WF-SIM, confocal, Airyscan, Lattice SIM, and now SIM² imaging illustrates how incremental improvements in optical sectioning and sub-diffraction structural discrimination progressively refine the interpretation of ATR.p-associated DNA damage response organization prior to final nanoscale interrogation using single-molecule STORM imaging workflows.

Image Correction

NONE

Image by J. H. Cheong
Image Analysis and Data Presentation by B.T. Bennett

© Copyright 2026 GMD12 LLC.

SOURCE PROVENANCE

Catalog	PA-RR-000013
Stage	SIM²
Instrument	ZEISS Elyra
Microscope configuration	Zeiss Elyra 5 Lattice SIM, AxioObserver.Z1/7 using Plan-Apochromat 63X/1.40 oil DIC M27, 1X Tubelens, was used with the following parameters for e
Structured source metadata values	53
Metadata source	PRESERVED_SOURCE_METHOD_PDF_TEXT
Cell model	HeLa
Image SHA-256	9864F2E3E683D7258040E13ECF4D6FA98F3ABFD092C0182FCD9D85D29586DD54
Method PDF SHA-256	5A4CC82C19100205F497D1FB3A0D4BBE03375B11072AB937EA194F5BC4C111B8

ORIGINAL IMAGE EVIDENCE / SINGLE-MOLECULE STORM

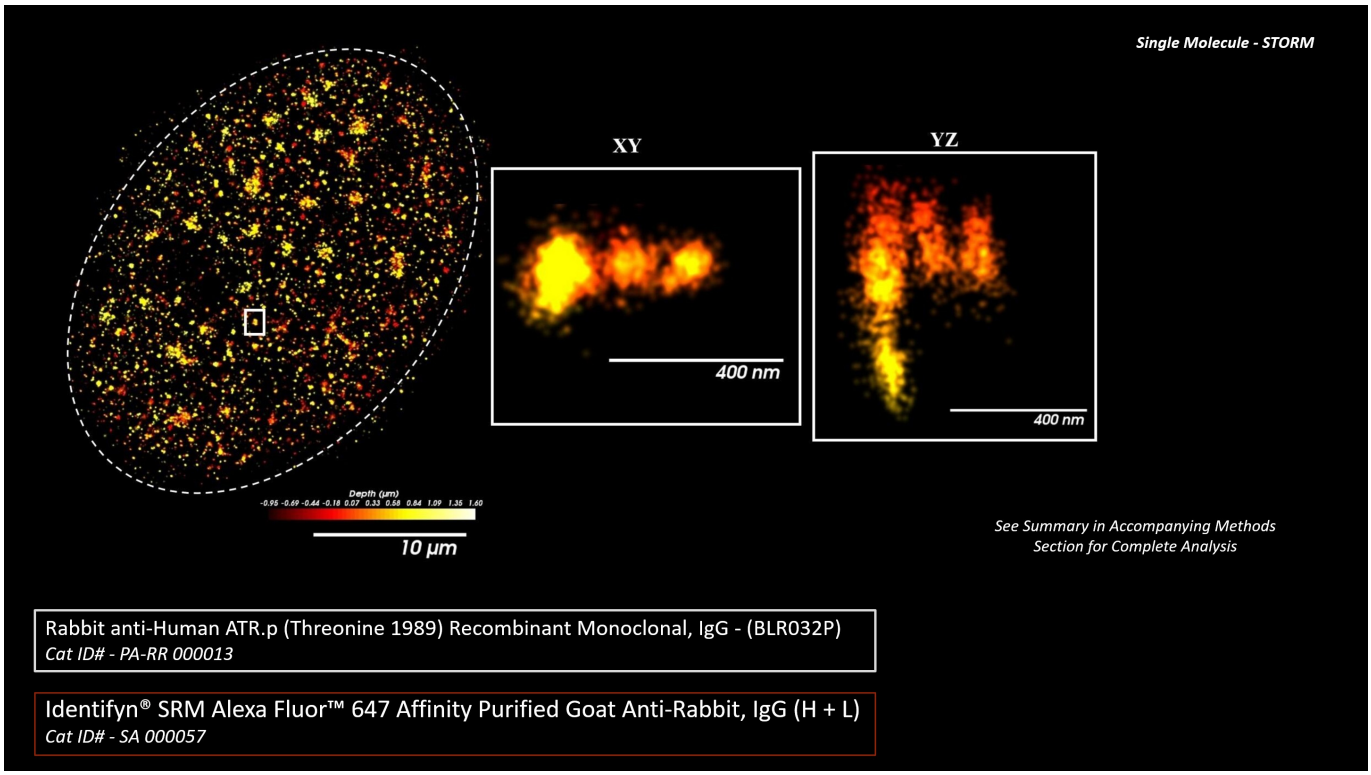

EVIDENCE TIER	Single-molecule STORM
INSTRUMENT	Bruker Vutara VXL
CELL MODEL	HeLa
DETECTED DYES	647
METADATA VALUES	79

STRUCTURED ACQUISITION METADATA / SINGLE-MOLECULE STORM

The values below were deterministically extracted from the preserved Identifyn method PDF text. They remain source-documented metadata, not new BENNETT measurements.

FIELD	SOURCE-DOCUMENTED VALUE
Platform / configuration	Bruker Vutara VXL Biplane Single Molecule Microscope, using an Olympus 60x/1.30 Silicon Oil objective, was used with the following parameters:
Objective	Olympus 60x/1.30 Silicon Oil objective
Number of Probes	1
Number of Simultaneous Probes	1
Number of Reference Probes	1
Camera	Both Cameras
Color Channel	Both Channels
Probe Capture Mode	Interleaved
Z -Stack Capture Mode	Interleaved
Multiple Location Capture	Not selected
Post Record Reference	Not Selected
Fluidics	Not Selected
Autofocus Drift Correction	On
Biplane Module	635 nm Dichroic
Objective	Silicon Selected
Stage Insert	Rectangular Selected
Coarse Focus Position	8-Well Chamber Selected
Dichroic	SuperRes
PSF	(Red, Orange)
Heater	Current: 26
Recording Vertical Field of View	100%
Widefield Camera Exposure Time	100 ms | 20 ms
Super Resolution Camera Exposure Time	20 ms
Widefield Camera Binning	1
Per-Probe Exposure Time	Selected
Predefined Probe	First probe: 640 nm (635 nm Dichroic); First reference probe: 640 nm (635 nm Dichroic)
Photoactivation/Imaging Laser	0% Selected
Exposure Time	20 ms Selected
Record Workflow	Selected Options
View Mode	Widefield 200 µm
Capture Mode	Live
Piezo Current	184.8 µm

FIELD	SOURCE-DOCUMENTED VALUE
Widefield 640nm	0.1X Neutral Density Filter: Selected, @ 0.2% Laser Input
Reference Probe 1 Laser control 640 nm (635 nm Dichroic)	Not Selected
Widefield camera Exposure Time	100 ms
Widefield Laser	"Widefield 640 nm" was deselected, and "calibrate" under Autofocus was selected.
Current Position	-0.979
Current Intensity	4.5
Calibration Value	-5070 nm/unit
Autofocus Mode	Pre-Capture
SuperRes	50 µm is selected
Piezo Record	Begin: 184; End: 184.8
SuperRes 640 nm	0.1X Neutral Density Filter: Selected, @ 0.02% Laser Input
Record Workflow - Record Tab	Capture Parameters
Frames	Probe 1: 200
Z Positions	4
Cycles	35
Time Points	1
Pause Between Cycles	Not Selected
Automatic Photoactivation Laser Control	Not Selected
Laser Power	30
Cutout Width	16 px
Max Frame Accumulation	1 frame
Max Accumulation Offset	1 px
Fiducial at Max Accumulation	Not selected
Max Particles Per Frame	No Max
Background SLPE Removal	Not Selected
Cutout/Background Removal	Not Selected
Preview Cutout Positions	Selected
Probe1	BG threshold: 15
Sizing Mode	Constant
Particle size	30 nm
Color by	Depth
Color Table	Single
Opacity Mode	Depth; Opacity 1: 0.55
Front-to-back Attenuation	Not Selected
Method	Particle (direct)

FIELD	SOURCE-DOCUMENTED VALUE
Time Intervals	10 Intervals
Pixel Size	50 nm
Smoothing	8.00
Radial precision	30
Axial precision	65
Clustering Algorithm	DBSCAN
Maximum Particle Distance	0.1 µm
Maximum Particle Count to Form Cluster	10
Compute Hulls	Not Selected
Compute Density Isosurfaces	Not Selected
Edit Settings	All Probes
Compute	Selected
Following Cluster Analysis Computation, under the Results Tab, ID Unassigned	Deselected

SOURCE METHOD

The text below is carried from the preserved Identifyn source record. Typography and pagination have been normalized for this preservation dossier; scientific wording has not been editorially rewritten.

Identifyn Standards for Optical Microscopy Methods™

Identifyn® Primary Antibody

Rabbit anti-Human ATR.p (Threonine 1989) Recombinant Monoclonal, IgG - (BLR032P)
Cat ID# - 000013

Identifyn® Secondary Antibody

Identifyn® SRM Alexa Fluor™ 647 Affinity Purified Goat Anti-Rabbit, IgG (H + L)
Cat ID# - SA 000057

ATR (Ataxia Telangiectasia and Rad3-related) is a critical serine/threonine kinase that plays a central role in the cellular response to DNA damage, particularly in response to replication stress and single-strand breaks (SSBs). Unlike ATM (Ataxia Telangiectasia Mutated), which is primarily activated by double-strand breaks, ATR is activated by persistent single-stranded DNA (ssDNA) regions that arise during DNA replication or repair processes.
Overview of ATR Activation

ATR is activated when extensive ssDNA accumulates, often resulting from stalled replication forks or other forms of replication stress. This activation is usually mediated by RPA (Replication Protein A), which binds to ssDNA and recruits ATR and its key activator, ATRIP (ATR Interacting Protein).

Recruitment to Sites of Damage: RPA-coated ssDNA signals DNA damage or replication stress. ATR, with ATRIP, is recruited to these sites, activating ATR's kinase activity.

Interaction with the 9-1-1 Complex: ATR activation is further facilitated by the 9-1-1 complex (comprising RAD9, RAD1, and HUS1), which is loaded onto DNA by RAD17-RFC at sites of DNA damage. This complex interacts with TOPBP1 (Topoisomerase II Binding Protein 1), a key activator of ATR, thereby fully activating ATR kinase activity.

ATR's Role in Single-Strand Break Repair

ATR plays a vital role in facilitating and coordinating the repair of single-strand breaks through various mechanisms:

Checkpoint Activation: ATR is critical for activating checkpoint signaling pathways, notably by phosphorylating CHK1. This leads to cell cycle arrest or delay, allowing time for DNA repair before cell division continues. This checkpoint activation is crucial in preventing cells from progressing with unrepaired single-strand breaks.

Coordination of Repair Pathways: ATR activation helps coordinate DNA repair processes by recruiting repair proteins and integrating signals across various pathways. This coordination ensures that repair proteins involved in base excision repair (BER), homologous recombination, and other SSB-related pathways are recruited and activated as needed.

Stabilization of Replication Forks: ATR contributes to the stabilization of stalled replication forks, preventing the collapse into double-strand breaks. This is particularly important in preventing the progression of single-strand breaks into more severe DNA damage.

ATR in DNA Damage Response

Beyond its direct role in facilitating single-strand break repair, ATR has broader implications in the DNA damage response:

Genomic Stability: By ensuring proper checkpoint activation and coordinating DNA repair, ATR helps maintain genomic stability, reducing the risk of mutations and chromosomal abnormalities.

Response to Replication Stress: ATR is particularly critical in responding to replication stress, which can result in single-strand breaks due to replication fork stalling or collapse. ATR's activation in these contexts ensures that DNA repair processes are promptly initiated.

ATR is a central player in responding to single-strand breaks and replication stress, activating checkpoint pathways, coordinating DNA repair, and stabilizing replication forks. Through these functions, ATR significantly contributes to maintaining genomic stability and ensuring that cells do not progress with unrepaired DNA damage.

Method

HeLa cells were grown on µ-Slide 8 Well high Glass Bottom Ibidi chamber. DNA damage was induced via treatment with 2 µM etoposide-spiked complete growth media for 48 hours, followed by -20 °C methanol fixation and blocked with Thermo Fisher Fish Serum Blocker cat#37527X3. The primary antibody, Rabbit anti-Human ATR.p (Threonine 1989) Recombinant Monoclonal, IgG - (BLR032P) was incubated for 1 hour at room temperature at a dilution of 1:100. Cells were washed 3X in Identifyn®'s proprietary Wash Buffer, and Identifyn® SRM Alexa Fluor™ 647 Affinity Purified Goat Anti-Rabbit, IgG (H + L) was incubated at room temperature for 1 hour at a dilution of 1:200. Cells were washed 5 times in Identifyn®'s proprietary Wash Buffer followed by the addition of Identifyn®'s proprietary STORM Buffer to the sample chamber enabling image acquisition.

Microscope

Bruker Vutara VXL Biplane Single Molecule Microscope, using an Olympus 60x/1.30 Silicon Oil objective, was used with the following parameters:

Calibration -

Calibration follows Identifyn®'s Calibration Standard Operating Procedure, which can be found here.

https://identifyn.com/storm-calibration

Image Acquisition -

SRX Software - Under the 'Single Molecule Localization' tab, 'Record' is selected and contains the following workflow tabs and parameters.

Configuration Tab - Capture Configuration

Number of Probes: 1
Number of Simultaneous Probes: 1
Number of Reference Probes: 1
Camera: Both Cameras
Color Channel: Both Channels
Probe Capture Mode: Interleaved
Z -Stack Capture Mode: Interleaved
Multiple Location Capture: Not selected
Post Record Reference: Not Selected
Fluidics: Not Selected
Autofocus Drift Correction: On

Microscope Configuration

Biplane Module: 635 nm Dichroic
Objective: Silicon Selected
Stage Insert: Rectangular Selected
Coarse Focus Position: 8-Well Chamber Selected
Dichroic: SuperRes
PSF: (Red, Orange)
Heater: Current: 26

Camera Configuration

Recording Vertical Field of View: 100%
Widefield Camera Exposure Time: 100 ms
Super Resolution Camera Exposure Time: 20 ms
Widefield Camera Binning: 1
Per-Probe Exposure Time: Selected

Probe Configuration

Predefined Probe: First probe: 640 nm (635 nm Dichroic); First reference probe: 640 nm (635 nm Dichroic)
Photoactivation/Imaging Laser: 0% Selected
Exposure Time: 20 ms Selected

Experiment Configuration

Record Workflow: Selected Options
View Mode: Widefield 200 µm
Capture Mode: Live

Stage and Piezo Selection

Examination of the Sample

Cell(s) or Cellular Structure Localization - The red-bordered box identifies the area of the SuperRes view and defines a suitable cell(s) or cellular structure. The cell(s) or structures are optimally focused.

Piezo Current: 184.8 µm

Probe 1 Laser control 640 nm (635 nm Dichroic)

Widefield 640nm: 0.1X Neutral Density Filter: Selected, @ 0.2% Laser Input
Reference Probe 1 Laser control 640 nm (635 nm Dichroic): Not Selected

Advanced Tools Option

Widefield camera Exposure Time: 100 ms
Default values are maintained unless otherwise noted.

Widefield Laser: "Widefield 640 nm" was deselected, and "calibrate" under Autofocus was selected.

Autofocus - Calibration Values

Current Position: -0.979
Current Intensity: 4.5
Calibration Value: -5070 nm/unit
Autofocus Mode: Pre-Capture

View Mode

SuperRes: 50 µm is selected

Capture Mode

Live

Stage and Piezo Selection

Cell(s) or Cellular Structure Localization - Positioning of the target Cell or Subsection of the Target Cell is optimized and optimally focused.

Piezo Record: Begin: 184; End: 184.8

Probe 1 Laser control 640 nm (635 nm Dichroic)

SuperRes 640 nm: 0.1X Neutral Density Filter: Selected, @ 0.02% Laser Input

Reference Probe 1 Laser control 640 nm (635 nm Dichroic)

Not Selected

Advanced Tools

Widefield Camera Exposure Time: 20 ms
Default values are maintained unless otherwise noted.

Record Workflow - Record Tab: Capture Parameters

Frames: Probe 1: 200
Z Positions: 4
Cycles: 35
Time Points: 1
Pause Between Cycles: Not Selected
Automatic Photoactivation Laser Control: Not Selected

Probe 1 Laser control 640 nm (635 nm Dichroic)

Laser Power: 30

Expert Configuration Options - The Localization Tab

Beyond the values shown, all other parameters were set to default values.

Localization

Cutout Width: 16 px
Max Frame Accumulation: 1 frame
Max Accumulation Offset: 1 px
Fiducial at Max Accumulation: Not selected
Max Particles Per Frame: No Max
Background SLPE Removal: Not Selected
Cutout/Background Removal: Not Selected
Preview Cutout Positions: Selected

Record Workflow - Localization Tab

Data Collection

The folder is created automatically with the localization file for this image acquisition.

Recording Summary

All parameters were carried over from previous tabs and are kept except:

Probe1: BG threshold: 15

Region of Interest -

Not selected

Display -

Was deployed to inspect if the BG threshold applied chooses localizations in an expected manner

Record Workflow - View Tab

Region of Interest

Default values

Visualization Parameters

Point Splatting
Sizing Mode: Constant
Particle size: 30 nm
Color by: Depth
Color Table: Single
Opacity Mode: Depth; Opacity 1: 0.55
Front-to-back Attenuation: Not Selected

Post Acquisition analysis - View Tab

Drift Correction - Computed with the following parameters:

Method: Particle (direct)
Time Intervals: 10 Intervals
Pixel Size: 50 nm
Smoothing: 8.00

Advanced Particle Filters - Applied to the drift-corrected data with the following parameters

Radial precision: 30
Axial precision: 65

The other parameters were not applied.

Statistical Analysis - Computed to clean low background signals.

Statistics Dialog - Cluster Analysis

Clustering Algorithm: DBSCAN

Parameters

Maximum Particle Distance: 0.1 µm
Maximum Particle Count to Form Cluster: 10
Compute Hulls: Not Selected
Compute Density Isosurfaces: Not Selected
Edit Settings: All Probes
Compute: Selected
Following Cluster Analysis Computation, under the Results Tab, ID Unassigned: Deselected

Summary

Panel A presents single-molecule STORM imaging of Rabbit anti-Human ATR.p (Threonine 1989) Recombinant Monoclonal, IgG - (BLR032P), visualized using Identifyn® SRM Alexa Fluor™ 647 Affinity Purified Goat Anti-Rabbit, IgG (H + L), following etoposide-induced DNA damage. Relative to conventional widefield, WF-SIM, confocal, Airyscan, Lattice SIM, and SIM² imaging, STORM microscopy provides substantially enhanced nanoscale spatial resolution and single-molecule localization precision, enabling direct visualization of highly discrete ATR.p-associated signaling architectures within the nuclear compartment. Structures previously observed as broad, punctate, or partially resolved sub-diffraction aggregates in prior modalities become increasingly distinguishable as heterogeneous nanoscale signaling domains with complex spatial organization.

The XY and orthogonal YZ reconstructions further illustrate the three-dimensional organization and depth-dependent distribution of ATR.p-associated signaling structures throughout the nuclear volume. Unlike preceding diffraction-limited or structured-illumination modalities, STORM imaging resolves highly localized substructures and heterogeneous nanoscale clustering patterns that were not fully distinguishable at lower imaging resolutions. Importantly, these findings demonstrate that many apparent single foci visualized by widefield, WF-SIM, confocal, Airyscan, Lattice SIM, and SIM² imaging likely represent composite signal territories composed of multiple underlying nanoscale structural domains.

Importantly, this dataset represents the terminal high-resolution stage of the Identifyn® Stepdown Methodology™, illustrating the progressive refinement of ATR.p-associated DNA damage response architecture across sequential imaging modalities. The transition from widefield through progressively higher-resolution optical and super-resolution workflows demonstrates how increasing spatial discrimination systematically refines the interpretation of ATR.p-associated signaling territories, culminating in single-molecule localization microscopy capable of resolving nanoscale organizational features not directly observable within preceding modalities. Despite the substantial improvement in structural resolution achieved by STORM imaging, additional molecular substructure likely remains below the modality's effective resolution limits, underscoring the continued inferential nature of structural interpretation even at the single-molecule scale.

Image by P. Raut

© Copyright 2026 GMD12 LLC.

SOURCE PROVENANCE

Catalog	PA-RR-000013
Stage	Single-molecule STORM
Instrument	Bruker Vutara VXL
Microscope configuration	Bruker Vutara VXL Biplane Single Molecule Microscope, using an Olympus 60x/1.30 Silicon Oil objective, was used with the following parameters:
Structured source metadata values	79
Metadata source	PRESERVED_SOURCE_METHOD_PDF_TEXT
Cell model	HeLa
Image SHA-256	ED07392482E90160D08CFA8BE4DF60BCD3DD79F37EEA8D41921DD720FF8C77C1
Method PDF SHA-256	5E6A554D67C3C60DC2F52A32B9FAA6149DE1B8F2A22F11325A9B3560F68D7AF5

ORIGINAL IMAGE EVIDENCE / CONTROL

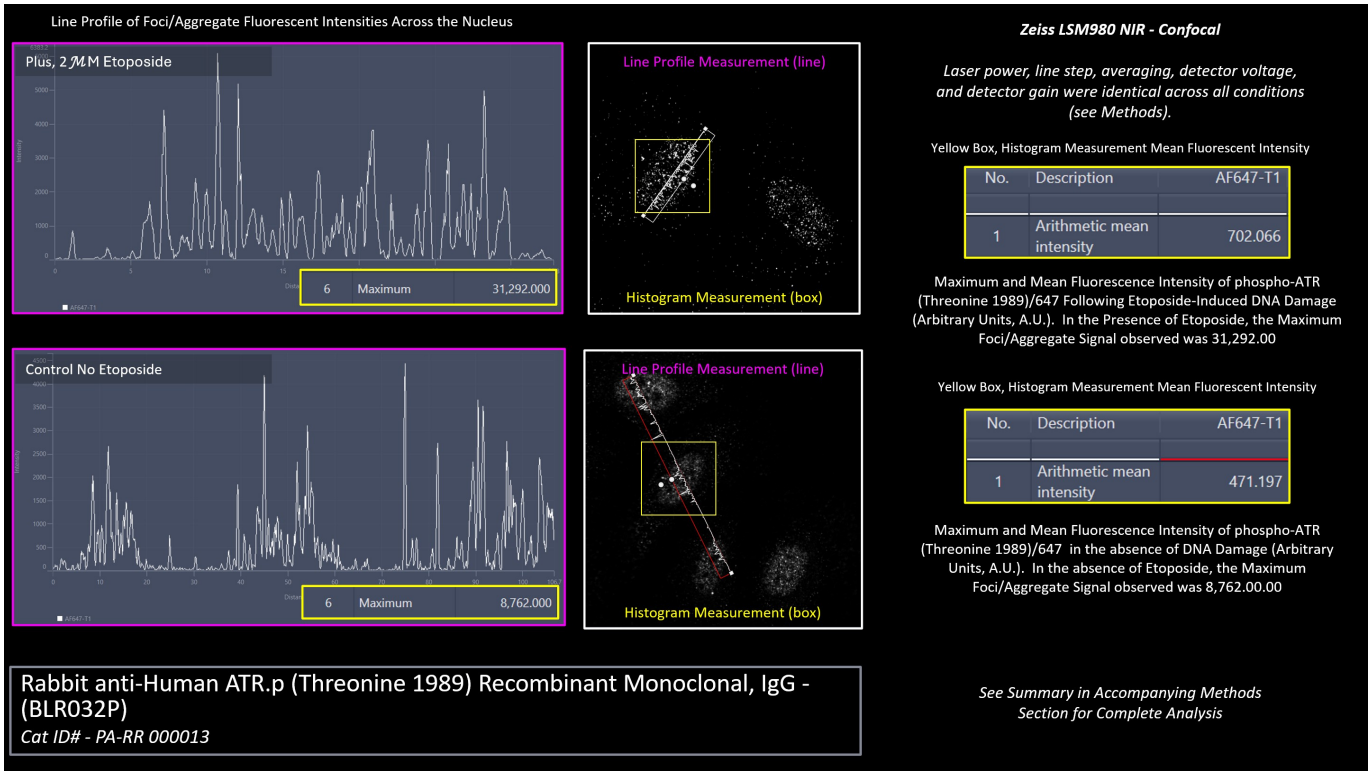

EVIDENCE TIER	Control
INSTRUMENT	ZEISS LSM 980
CELL MODEL	HeLa
DETECTED DYES	405/DAPI; 488; 647
METADATA VALUES	55

STRUCTURED ACQUISITION METADATA / CONTROL

The values below were deterministically extracted from the preserved Identifyn method PDF text. They remain source-documented metadata, not new BENNETT measurements.

FIELD	SOURCE-DOCUMENTED VALUE
Platform / configuration	Zeiss LSM980 Confocal with NIR Detection, Axio Observer.Z1/7, using a Plan-Apochromat 63x/1.40 Oil DIC M27, was used with the following parameters for each dye:
Objective	Plan-Apochromat 63x/1.40 Oil DIC M27
Z-Stack	151 Slices (4.5 µm)
Channels	1
Scaling (Per Pixel)	0.059 µm X 0.059 µm X 0.030 µm | 0.059 µm X 0.059 µm
Image Size (Pixels)	1407 X 1407 | 2266 X 2266
Image Size (Scaled)	82.77 µm X 82.77 µm | 133.28 µm X 133.28 µm
Bit Depth	16 Bit
Image Center Position	X: 91.51 mm, Y: 49.99 mm | X: 91.24 mm, Y: 48.00 mm
Stage Position	X: 91.51 mm, Y: 49.99 mm | X: 91.24 mm, Y: 48.00 mm
ROI Center Offset	X: 0.00 µm, Y: 0.00 µm
Reflector	None
Contrast Method	Fluorescence
Pinhole	1.00 AU / 64 µm
LMS MBS	MBS 488/639 & 405/730
LMS SBS	SBS SP 615
Laser Wavelength	639 nm @ 1.8%
Laser Blanking	Enabled
Scan Mode	Frame
Scan Zoom	1.6 | 1.0
Rotation	0°
Sampling	1.20
Pixel Time	0.28 µs | 0.23 µs
Frame Time	5.28 s | 11.26 s
LSM Scan Speed	11 | 9
Scan Direction	Bidirectional
Line Step	1
Averaging	8
Excitation Wavelength	653
Emission Wavelength	668
Effective NA	1.4
Detection Wavelength	647 - 700 | 640 - 732
Imaging Device	GaAsP-Pmt3

FIELD	SOURCE-DOCUMENTED VALUE
Detector Type	GaAsP-PMT
Detector Gain	550 V
Detector Offset	0
Detector Digital Gain	1.0
LSM Plus Mode	Filter: 8.6 (3D, Auto) | Filter: 8.2 (3D, Auto)
Profile Definition	Stroke Thickness 1.5, Normal View, Grid Distance 1
Profile View	X and Y axes were set to Auto - X (Min 0.0 and Max 32.80), Y (Min 0.0 and Max 6383) | X and Y axes were set to Auto - X (Min 0.0 and Max 106.7), Y (Min 0.0 and Max 4653)
Histogram Definition	Normal, Histo Table set to Frequency, Bin Count 256, Bin Size was 256, Lower Threshold 0, Upper Threshold 65535
Histogram View	X and Y axes were set to Auto - X (Min 0.0 and Max 65535), Y (Min 0.0 and Max 100000) | X and Y axes were set to Auto - X (Min 0.0 and Max 65535), Y (Min 0.0 and Max 200000)
Arithmetic Mean intensity	702.066 | 471.197

SOURCE METHOD

The text below is carried from the preserved Identifyn source record. Typography and pagination have been normalized for this preservation dossier; scientific wording has not been editorially rewritten.

Identifyn Standards for Optical Microscopy Methods™

Identifyn® Primary Antibody

Rabbit anti-Human ATR.p (Threonine 1989) Recombinant Monoclonal, IgG - (BLR032P)
Cat ID# - 000013

Identifyn® Secondary Antibody

Identifyn® SRM Alexa Fluor™ 647 Affinity Purified Donkey Anti-Rabbit, IgG (H + L)
Cat ID# - SA 000060

ATR (Ataxia Telangiectasia and Rad3-related) is a critical serine/threonine kinase that plays a central role in the cellular response to DNA damage, particularly in response to replication stress and single-strand breaks (SSBs). Unlike ATM (Ataxia Telangiectasia Mutated), which is primarily activated by double-strand breaks, ATR is activated by persistent single-stranded DNA (ssDNA) regions that arise during DNA replication or repair processes.
Overview of ATR Activation

ATR is activated when extensive ssDNA accumulates, often resulting from stalled replication forks or other forms of replication stress. This activation is usually mediated by RPA (Replication Protein A), which binds to ssDNA and recruits ATR and its key activator, ATRIP (ATR Interacting Protein).

Recruitment to Sites of Damage: RPA-coated ssDNA signals DNA damage or replication stress. ATR, with ATRIP, is recruited to these sites, activating ATR's kinase activity.

Interaction with the 9-1-1 Complex: ATR activation is further facilitated by the 9-1-1 complex (comprising RAD9, RAD1, and HUS1), which is loaded onto DNA by RAD17-RFC at sites of DNA damage. This complex interacts with TOPBP1 (Topoisomerase II Binding Protein 1), a key activator of ATR, thereby fully activating ATR kinase activity.

ATR's Role in Single-Strand Break Repair

ATR plays a vital role in facilitating and coordinating the repair of single-strand breaks through various mechanisms:

Checkpoint Activation: ATR is critical for activating checkpoint signaling pathways, notably by phosphorylating CHK1. This leads to cell cycle arrest or delay, allowing time for DNA repair before cell division continues. This checkpoint activation is crucial in preventing cells from progressing with unrepaired single-strand breaks.

Coordination of Repair Pathways: ATR activation helps coordinate DNA repair processes by recruiting repair proteins and integrating signals across various pathways. This coordination ensures that repair proteins involved in base excision repair (BER), homologous recombination, and other SSB-related pathways are recruited and activated as needed.

Stabilization of Replication Forks: ATR contributes to the stabilization of stalled replication forks, preventing the collapse into double-strand breaks. This is particularly important in preventing the progression of single-strand breaks into more severe DNA damage.

ATR in DNA Damage Response

Beyond its direct role in facilitating single-strand break repair, ATR has broader implications in the DNA damage response:

Genomic Stability: By ensuring proper checkpoint activation and coordinating DNA repair, ATR helps maintain genomic stability, reducing the risk of mutations and chromosomal abnormalities.

Response to Replication Stress: ATR is particularly critical in responding to replication stress, which can result in single-strand breaks due to replication fork stalling or collapse. ATR's activation in these contexts ensures that DNA repair processes are promptly initiated.

ATR is a central player in responding to single-strand breaks and replication stress, activating checkpoint pathways, coordinating DNA repair, and stabilizing replication forks. Through these functions, ATR significantly contributes to maintaining genomic stability and ensuring that cells do not progress with unrepaired DNA damage.

Method

Plus Damage -

HeLa cells were grown on acid-etched #1.5H cover glass to ~50% confluency. DNA damage was induced via treatment with 2 µM etoposide-spiked complete growth media for 24 hours, followed by -20 °C methanol fixation and blocked with Thermo Fisher Fish Serum Blocker cat#37527X3. The primary antibody, Rabbit anti-Human ATR.p (Threonine 1989) Recombinant Monoclonal, IgG - (BLR032P), was incubated for 1 hour at room temperature at a dilution of 1:250. Cells were washed 3X in PBS. Identifyn® SRM Alexa Fluor™ 647 Affinity Purified Donkey Anti-Rabbit, IgG (H + L) was incubated at room temperature for 1 hour at a dilution of 1:1000. Cells were washed 5 times in 1X PBS and mounted using ProLong™ Diamond Antifade Mountant with DAPI (cat# P36962).

Minus Damage -

HeLa cells were grown on acid-etched #1.5H cover glass to ~50% confluency, then fixed in -20 °C methanol and blocked with Thermo Fisher Fish Serum Blocker (cat#37527X3). The primary antibody, Rabbit anti-Human ATR.p (Threonine 1989) Recombinant Monoclonal, IgG - (BLR032P), was incubated for 1 hour at room temperature at a dilution of 1:250. Cells were washed 3 times in 1X PBS. Identifyn® SRM Alexa Fluor™ 647 Affinity Purified Donkey Anti-Rabbit, IgG (H + L) was incubated at room temperature for 1 hour at a dilution of 1:1000. Cells were washed 5 times in 1X PBS and mounted using ProLong™ Diamond Antifade Mountant with DAPI (cat# P36962).

Microscope

Zeiss LSM980 Confocal with NIR Detection, Axio Observer.Z1/7, using a Plan-Apochromat 63x/1.40 Oil DIC M27, was used with the following parameters for each dye:

Z Stack - (3D) - 2D at Z-Plane 77 of 151, Panel A, from Confocal Data Set

Z-Stack = 151 Slices (4.5 µm)

Channels = 1
Scaling (Per Pixel) = 0.059 µm X 0.059 µm X 0.030 µm
Image Size (Pixels) = 1407 X 1407
Image Size (Scaled) = 82.77 µm X 82.77 µm
Bit Depth = 16 Bit
Image Center Position = X: 91.51 mm, Y: 49.99 mm
Stage Position = X: 91.51 mm, Y: 49.99 mm
ROI Center Offset = X: 0.00 µm, Y: 0.00 µm

Single Plane (2D) - Control

Channels = 1
Scaling (Per Pixel) = 0.059 µm X 0.059 µm
Image Size (Pixels) = 2266 X 2266
Image Size (Scaled) = 133.28 µm X 133.28 µm
Bit Depth = 16 Bit
Image Center Position = X: 91.24 mm, Y: 48.00 mm
Stage Position = X: 91.24 mm, Y: 48.00 mm
ROI Center Offset = X: 0.00 µm, Y: 0.00 µm

647 - Plus Damage, from Confocal Data Set

Reflector = None
Contrast Method = Fluorescence
Pinhole = 1.00 AU / 64 µm
LMS MBS = MBS 488/639 & 405/730
LMS SBS = SBS SP 615
Laser Wavelength = 639 nm @ 1.8%
Laser Blanking = Enabled
Scan Mode = Frame
Scan Zoom = 1.6
Rotation = 0°
Sampling = 1.20
Pixel Time = 0.28 µs
Frame Time = 5.28 s
LSM Scan Speed = 11
Scan Direction = Bidirectional
Line Step = 1
Averaging = 8
Excitation Wavelength = 653
Emission Wavelength = 668
Effective NA = 1.4
Detection Wavelength = 647 - 700
Imaging Device = GaAsP-Pmt3
Detector Type = GaAsP-PMT
Detector Gain = 550 V
Detector Offset = 0
Detector Digital Gain = 1.0
LSM Plus Mode = Filter: 8.6 (3D, Auto)

647 - Minus Damage - noting the same laser input power and conditions

Reflector = None
Contrast Method = Fluorescence
Pinhole = 1.00 AU / 64 µm
LMS MBS = MBS 488/639 & 405/730
LMS SBS = SBS SP 615
Laser Wavelength = 639 nm @ 1.8%
Laser Blanking = Enabled
Scan Mode = Frame
Scan Zoom = 1.0
Rotation = 0°
Sampling = 1.20
Pixel Time = 0.23 µs
Frame Time = 11.26 s
LSM Scan Speed = 9
Scan Direction = Bidirectional
Line Step = 1
Averaging = 8
Excitation Wavelength = 653
Emission Wavelength = 668
Effective NA = 1.4
Detection Wavelength = 640 - 732
Imaging Device = GaAsP-Pmt3
Detector Type = GaAsP-PMT
Detector Gain = 550 V
Detector Offset = 0
Detector Digital Gain = 1.0
LSM Plus Mode = Filter: 8.2 (3D, Auto)

Profile View Display - Plus DNA Damage, Top

Profile Definition = Stroke Thickness 1.5, Normal View, Grid Distance 1

Profile View = X and Y axes were set to Auto - X (Min 0.0 and Max 32.80), Y (Min 0.0 and Max 6383)

This panel measures phospho-ATR DNA damage-induced foci/aggregates across an arbitrary line, noting that the foci/aggregate signal reached approximately ~7K A.U. at its maximum.

Measured at the Z-plane 77 of 151.

Profile View Display - Minus DNA Damage, Bottom

Profile Definition = Stroke Thickness 1.5, Normal View, Grid Distance 1

Profile View = X and Y axes were set to Auto - X (Min 0.0 and Max 106.7), Y (Min 0.0 and Max 4653)

This panel measures phospho-ATR in the absence of DNA damage across an arbitrary line, noting that the foci/aggregate signal reached approximately ~4K A.U. at its maximum.

Histogram Display - Plus DNA Damage, Top

Histogram Definition = Normal, Histo Table set to Frequency, Bin Count 256, Bin Size was 256, Lower Threshold 0, Upper Threshold 65535

Histogram View = X and Y axes were set to Auto - X (Min 0.0 and Max 65535), Y (Min 0.0 and Max 100000)

Arithmetic Mean intensity = 702.066

The histogram was generated from the yellow-boxed region to quantify the overall phospho-ATR protein response within a defined nuclear area following DNA damage induction. This measurement provides additional support for the observed increase in signal relative to the control condition, complementing the line-profile analysis presented alongside it.

Histogram Display - Minus DNA Damage, Bottom

Histogram Definition = Normal, Histo Table set to Frequency, Bin Count 256, Bin Size was 256, Lower Threshold 0, Upper Threshold 65535

Histogram View = X and Y axes were set to Auto - X (Min 0.0 and Max 65535), Y (Min 0.0 and Max 200000)

Arithmetic Mean intensity = 471.197

The histogram was generated from the yellow-boxed region to quantify the overall phospho-ATR protein within a defined nuclear area in the absence of DNA damage induction. This measurement provides additional support for the observed increase in signal relative to the control condition, complementing the line-profile analysis presented alongside it.

Control Conclusion -

In the absence of DNA damage, ATR.p (647) exhibited a predominantly low-intensity, diffuse nuclear distribution with minimal focal organization, consistent with basal ATR signaling activity under unstressed cellular conditions. Following etoposide-induced DNA damage, ATR.p exhibited a pronounced increase in fluorescence intensity, along with extensive reorganization into discrete intranuclear foci and higher-order, aggregate-like signaling territories. Quantitative profile-view analysis revealed peak signal intensities approaching ~7K A.U. in the DNA-damaged condition compared to ~4K A.U. in the untreated control. In contrast, histogram analysis showed a substantial increase in the arithmetic mean fluorescence intensity after DNA damage induction.

The observed transition from diffuse low-intensity nuclear staining to highly organized punctate ATR.p-associated signaling architectures is strongly consistent with canonical ATR activation in response to replication stress and DNA damage. These findings support recruitment of activated ATR signaling complexes to RPA-coated single-stranded DNA regions and engagement of downstream DNA damage response (DDR) checkpoint pathways. Importantly, the marked increase in signal intensity, focal organization, and aggregate complexity observed under DNA-damaged conditions remained highly consistent across the sequential workflows of widefield, WF-SIM, confocal, Airyscan, Lattice SIM, SIM², and STORM imaging, further supporting the biological specificity, reproducibility, and structural coherence of the ATR.p-associated DNA damage response observed throughout the Identifyn® Stepdown Methodology™ progression.

Collectively, these findings support the performance and biological specificity of Rabbit anti-Human ATR.p (Threonine 1989) Recombinant Monoclonal, IgG - (BLR032P) across multiple orthogonal imaging modalities and resolution scales. The antibody demonstrated robust signal generation, biologically coherent DNA damage-dependent redistribution, strong preservation of subcellular localization characteristics, and reproducible structural behavior throughout progressively higher-resolution imaging workflows. The combined control, quantitative, and multimodal imaging datasets support the utility of BLR032P as a high-performance research reagent for investigating ATR-associated replication stress signaling and DNA damage response biology under both conventional fluorescence and advanced super-resolution imaging conditions.

Image Corrections

NONE

Image by J.K. Bennett
Image Analysis and Data Presentation by B.T. Bennett
© Copyright 2026 GMD12 LLC.

SOURCE PROVENANCE

Catalog	PA-RR-000013
Stage	Control
Instrument	ZEISS LSM 980
Microscope configuration	Zeiss LSM980 Confocal with NIR Detection, Axio Observer.Z1/7, using a Plan-Apochromat 63x/1.40 Oil DIC M27, was used with the following paramete
Structured source metadata values	55
Metadata source	PRESERVED_SOURCE_METHOD_PDF_TEXT
Cell model	HeLa
Image SHA-256	20E36AE7697461E676452B6EA817C033029AB55E313D778A5584F9006F785E75
Method PDF SHA-256	E290CA0D4DA9D7001EA23750FFA066DDB5589CC25C321BF987FDC514CF95BABD